Obtaining reactor-relevant divertor conditions in tokamaks

2011 Nucl. Fusion 51 063001

(http://iopscience.iop.org/0029-5515/51/6/063001)

IOP Publishing and International Atomic Energy Agency Nuclear Fusion
Nucl. Fusion **51** (2011) 063001 (16pp) doi:10.1088/0029-5515/51/6/063001

Obtaining reactor-relevant divertor conditions in tokamaks

P.C. Stangeby[1] **and A.W. Leonard**[2]

[1] University of Toronto Institute for Aerospace Studies, Toronto, M3H 5T6, Canada
[2] General Atomics, PO Box 85608, San Diego, CA 92186-5608, USA

E-mail: stangeby@fusion.gat.com

Received 1 October 2010, accepted for publication 22 March 2011
Published 28 April 2011
Online at stacks.iop.org/NF/51/063001

Abstract
It is argued that the paramount boundary plasma issue for DT reactors is likely to be the erosion wear of the plasma facing components, PFCs, and that a number of potential solutions all require the achievement of not only low temperature ($\lesssim$10 eV) but also high density ($\gtrsim 10^{21}$ m^{-3}) in the divertor. Estimates are made of the minimum heating power, P_{heat}, required to achieve a divertor target temperature of $T_t = 5$ eV and density $n_t > 10^{21}$ m^{-3}, based on four recent hypotheses or scalings for the width of the power footprint on the target, λ_{qt}. Each of these result in predictions of how the required minimum P_{heat} depends on device size, namely as R, $R^{3/2}$ or R^2. The absolute magnitude for the required values of minimum P_{heat} is found not to vary significantly among the four power scalings; for the most part a factor of order ~2 for a significant range of R. The four hypotheses/scalings for λ_{qt} are empirically based; however, they draw on measurements made in tokamaks that did not have divertors operating primarily under these conditions. In order to establish if any of these power scalings are applicable, they are compared with measurements from a set of DIII-D discharges with high $n_t \sim 0.35 \times 10^{21}$ at 5 eV. It is found that all four power scalings match the experimental measurements to within the uncertainties. The main objective is to determine what power is needed to achieve the required divertor conditions in future devices, for both reactor and simulator tokamaks, and therefore the approximate agreement of the four, strongly empirical, power scalings increases confidence that this may be possible.

1. Introduction

It is desirable to be able to study boundary processes that are expected to be important in DT magnetic fusion reactors in current tokamaks and in *experimental simulator tokamaks* at reduced scale and reduced cost. This leads to a number of basic questions:

(a) What are the paramount boundary issues for DT reactors requiring solution?
(b) What boundary, e.g. divertor, plasma conditions have to be created in (i) reactors, (ii) simulators, in order to achieve potentially viable solutions for reactors and to enable reactor-relevant research to be performed in simulators?
(c) Do the plasma conditions required for reactors have to be matched absolutely in simulators or can they be scaled, potentially with cost savings?
(d) For a specified device size (major radius R) how much heating power, P_{heat}, is required to achieve the required plasma conditions in the divertor, i.e. what is the *power-scaling law* so far as tokamak boundary issues are concerned?

A case is presented in section 2 that the paramount boundary plasma issue for DT reactors is likely to be the erosion wear of the plasma facing components, PFCs, and that a number of potential solutions all require the achievement of not only low temperature ($\lesssim$10 eV) but also high density ($\gtrsim 10^{21}$ m^{-3}) in the divertor. Fortunately, these divertor conditions are not incompatible with the ones required to solve other critical boundary issues such as heat flux control and He-ash removal by pumping; indeed they are generally beneficial.

In section 3 simple conservation models are used to show that, for specified divertor density and temperature, the resulting values of density and temperature 'upstream', i.e. at the separatrix adjacent to the confined plasma, are insensitive to the tokamak size, major radius R. Therefore in any DT *power reactor* tokamak, independent of size, the boundary (separatrix) conditions for the confined plasma will be approximately the same. (This does not necessarily hold for *experimental simulator tokamaks*, as will be discussed.)

In section 4 a similar, simple modelling is used to estimate the heating power, P_{heat}, required to achieve the divertor plasma conditions identified in section 2. This analysis encounters a major uncertainty, namely the physics controlling the power width at the divertor target, λ_{qt}; there are appreciable uncertainties in even how it scales, e.g. with R, P_{heat}, density,

plasma current, etc. Four recent hypotheses and scalings for λ_{qt} are used here, together with two-point modelling of the divertor and scrape-off layer (SOL), resulting in different predictions of how the required P_{heat} depends on R, namely as R, $R^{3/2}$ or R^2.

These hypotheses and scalings for λ_{qt} are empirically based, drawing primarily on measurements made in tokamaks that did not have divertors operating in the very high density, cold regime of interest here. It is therefore not clear that any of them are appropriate for present purposes. Comparisons are therefore needed of these different scalings with measurements in well-diagnosed divertors operating in this regime or as close to it as possible. Section 5 discusses the problem of acquiring sufficient experimental information from present divertor experiments to constrain even the simple power-scaling models of section 4 in order to be able to establish if any of them are applicable and if possible to distinguish among the different hypotheses/scalings for λ_{qt}.

In section 6 measurements made in a set of high-power, high-density, lower single-null DIII-D discharges, where the 2D spatial distribution of n_e and T_e were mapped throughout the outer divertor to locations above the X-point using Thomson scattering, are shown to be (just) adequate to constrain the simple modelling in section 4. It is found that all four power scalings agree with the measured values of the power into the outer leg of the SOL, $P_{SOL}^{outer\text{-}leg}$, to within a factor of ~2 or so for the three discharges analysed, which is well within the combined uncertainties of the scalings and the experimental measurements. From this two conclusions are reached:

(a) Even though the four power scalings are based largely on experimental results for divertors that were significantly less dense and typically hotter than is of interest here, they have been found to also agree to within experimental uncertainties with the well-diagnosed DIII-D discharges which had divertor conditions close to those of interest.

(b) Since the combined uncertainties are at least a factor of 2 it is not possible to discriminate amongst the four scalings of λ_{qt} on the basis of this initial test. While it may not be possible to determine the best λ_{qt}-scaling, the important objective is to know what power is needed to achieve the required divertor conditions in future devices, for both reactor and simulator tokamaks. The approximate agreement of the four power scalings increases confidence that this may be possible.

In section 7 the question is addressed of whether an *experimental simulator tokamak* needs to match absolutely the divertor density and temperature required in a DT power reactor, or whether scaling is possible. It is concluded that divertor temperature has to be matched absolutely—in agreement with earlier divertor scaling studies [1, 2]—but that the required divertor density scales with magnetic field B. Thus a lower divertor density together with a lower B can replicate the conditions required for studying the critical reactor-relevant erosion-wear issue in an *experimental simulator tokamak*, which may permit cost savings.

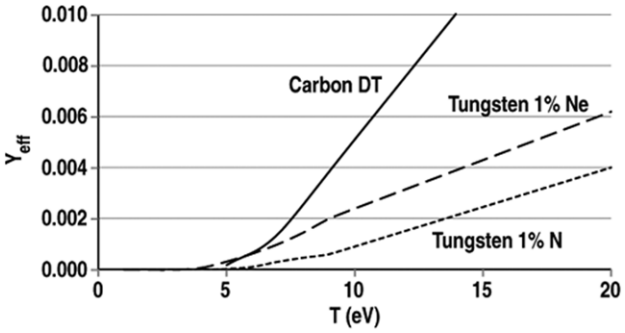

Figure 1. Effective physical sputtering yields based on TRIM code calculations of Eckstein [8]. For carbon sputtering (solid line) the impacting ions are assumed to be 50 : 50 D : T, $T_e = T_i$ and impact energy $E_{imp} \sim 5\,kT$. For tungsten the sputtering is due to low-Z radiating impurities seeded into the plasma at an assumed 1% level: Ne (long dashes), N (short dashes). Details are given in the appendix.

2. Divertor temperature and density required in a DT tokamak power reactor for acceptable lifetime of the PFCs

The window of practical interest for the plasma temperature at the divertor target, T_t, of a DT tokamak fusion power reactor may be rather small. For $T_t \gtrsim 10$ eV, sputtering yields increase rapidly, see figure 1, probably making this operating condition impractical. It is also the case that P_{rad}-cooling by low-Z radiators is most effective for rather cold divertors; the maximum in the radiating efficiency for N, for example, occurs at $T \sim 11$ eV [3].

At the colder end of practical interest, namely for $T_t \lesssim 2$ eV, the divertor is detached or close to detaching which can make it difficult to maintain good confinement, see e.g. the discussion in appendix A of [4]. It therefore appears that DT power reactor tokamaks may have to operate with divertor temperatures within a factor of ~2 of ~5 eV.

It will be argued here that the divertor density, n_t, also has to satisfy a constraint, namely $n_t \gtrsim 10^{21}\,m^{-3}$, in order to avoid rapid destruction of the divertor targets in a reactor by sputtering erosion. In present devices erosion wear is unimportant because the integrated annual ionic fluence onto the PFCs is relatively small and therefore the associated eroded material loss is small. In power reactors, however, the integrated annual ionic fluence to the PFCs will increase by ~5 orders of magnitude compared with present devices, see table 1. This is a much greater increase in operational regime than is involved in almost any other aspect required for the development of practical magnetic fusion energy.

Plasma–wall interaction, PWI, in present devices usually does so little to the PFC material that very sensitive surface measurements are required to even detect the effects. In power reactors, however, the PWI will strongly 'work' the PFC material, (re-)creating the wall material that the plasma reacts with. Table 1 gives rough estimates of the rate at which the PFC material is 'worked', i.e. the gross erosion rate, in present and future devices. The rates are in kg per calendar (not run) year. The numbers in table 1 assume $P_{rad} = 75\% P_{heat}$, thus $0.25 P_{heat} = \gamma k T_t \phi_t$, where γ = sheath heat transmission coefficient = 7, see e.g. section 25.5 of [5]; T_t = plasma

Table 1. A rough estimate of the rate at which plasma 'works' the PFC material in present and future devices assuming $T = 10\,\mathrm{eV}$ for the plasma in contact with the PFC material. Material circulation rate ≡ gross erosion rate $= \phi_t Y_{\mathrm{eff}}$ = the rate at which the plasma works the material. It is assumed that 100% of the PFCs are made of (or are coated with) either Be, B, C or W. See text for a discussion of the other assumptions used to calculate the values in this table.

Device	P_{heat} (MW)	Annual run time (s/year)	Fluence of D/T ions to surfaces (TC/yr)[a]	Beryllium circulation rate (kg/yr)	Boron circulation rate (kg/yr)	Carbon circulation rate (kg/yr)	Tungsten circulation rate (kg/yr)
DIII-D	20	10^4	0.0007	2.8	1	0.5	0.7
JT-60SA	34	10^4	0.0017	4.8	1.7	0.9	1.2
EAST	24	10^5	0.01	34	11	5	8
ITER	100	10^6	0.4	1680	580	270	410
FDF	100	10^7	3	13 400	4600	2100	3300
Reactor	400	2.5×10^7	40	141 000	50 000	22 000	31 000

[a](tera-coulombs/year).

temperature in contact with PFC surfaces; ϕ_t = total D/T-ion flux to all surfaces (ions/s), targets and walls. For illustration a value of $T_t = 10\,\mathrm{eV}$ has been used in table 1 for devices, present and future. Although in present devices a value of $T_t = 10\,\mathrm{eV}$ is on the low side for typical operating conditions, if this were the condition in a reactor the gross erosion rates would be enormous, many tons per year, whether for low-Z, e.g. C, or high-Z, e.g. W, targets.

For completeness low-Z materials are also considered as they may potentially be employed to advantage as coatings on substrates which are resistant to neutron damage [6, 7]. For the physical sputtering of Be and B the same assumptions were used as for C in figure 1 and the appendix; effective sputtering yield Y_{eff} (Be/B/C) = 0.042/0.012/0.005 [8]. For reasons of thermal efficiency reactors will operate with very hot walls, see e.g. [9]. Carbon chemical sputtering and radiation-enhanced sublimation, RES, are not significant at the assumed C surface temperature of ∼1000 °C; see e.g. section 3.3 of [5]. Tungsten sputtering is assumed to be due to 0.5% nitrogen radiating additive, Y_{eff} (W) = 0.000 45, figure 1, see the appendix also. The material circulation rate or *gross* erosion rate is not to be confused with the *net* erosion rate, which is the required (external) refurbishment rate. The latter quantity is smaller—in fact it is probably essential that it be made enormously smaller—than the first one because a significant amount of the sputtered material can re-deposit locally.

No attempt has been made here, table 1, to estimate the spatial distribution of the gross erosion pattern on the PFC surfaces, e.g. at the divertor strike points. This would require knowledge of how to scale power and particle widths, about which there is currently significant uncertainty. However, the uncertainty factor involved in these widths is insignificant compared with the scaling up factor of ∼5 orders of magnitude for the annual fluence of D/T ions to PFC surfaces. Thus, based on the crude assumptions made in table 1, the rate of gross erosion at the strike points of a power reactor would be roughly ∼5 orders of magnitude higher than that experienced in present day experimental devices. The measured rate of *net* erosion in present devices is 0.1–10 nm s^{-1} [10], thus for a typical 10^4 s/year operation in present devices, the rate of surface recession at the divertor strike points is only $\sim10^{-6}$–10^{-4} m/year. However, if net erosion also were to scale up by ∼5 orders of magnitude then for reactors the rate of recession of the targets would be 0.1–10 m/year which is clearly intolerable, certainly for conventional, i.e. infrequently replaced, PFCs, and probably even for continuously *in situ* refurbished coated PFCs.

Power reactors must suppress net erosion by an extremely large factor relative to what has been achieved in existing experimental devices. It is essential therefore that a means be found for breaking the connection between the ionic outflux to PFCs and the erosion wear of the PFCs. This can, in principle, be achieved in a number of ways:

(a) There is a small temperature window between divertor detachment, which occurs for $T_t < T_t^{\mathrm{det}} \sim 1$–$2\,\mathrm{eV}$, and the sputtering threshold temperature, $T_t < T_t^{\mathrm{sput\text{-}thresh}} \sim 3$–$5\,\mathrm{eV}$, where the ions incident on the PFCs have an impact energy E_{impact} less than the threshold for physical sputtering. It is shown in the appendix that for Be + D/T, $T_t^{\mathrm{sput\text{-}thresh}} \sim 2\,\mathrm{eV}$; for B + D/T and C + D/T, $T_t^{\mathrm{sput\text{-}thresh}} \sim 4.5\,\mathrm{eV}$; for W + N, $T_t^{\mathrm{sput\text{-}thresh}} \sim 4\,\mathrm{eV}$; and for W + Ne, $T_t^{\mathrm{sput\text{-}thresh}} \sim 3\,\mathrm{eV}$. Therefore, by operating the divertor in this narrow temperature window, $T_t^{\mathrm{det}} < T_t < T_t^{\mathrm{sput\text{-}thresh}}$, it is possible, in principle, to eliminate physical sputtering almost entirely. As noted, for reasons of thermal efficiency, reactors will operate with very hot walls, e.g. ∼1000 °C, in which case the chemical sputtering of carbon is negligible. Thus operation in this temperature window—whether with low-Z-coated or tungsten divertor targets—could in principle avoid erosion wear of the targets, despite the extremely high integrated annual ionic fluence onto the PFCs.

(b) Although, as noted above, experience to date has shown that operation with $T_t < T_t^{\mathrm{det}}$ encounters issues regarding core plasma performance and control of the plasma, further research may discover ways to avoid the disadvantages while enjoying the advantages of such cold divertor operation—the most important of which would, like for (a), be the possibility of complete avoidance of erosion wear of the divertor PFCs. Recently, innovative divertor magnetic designs have been proposed, super-X [11] and snow-flake [12], which could provide opportunities of exploiting detachment with good control and without degradation of core plasma performance. When both divertors are detached in DIII-D, the entire divertor experiences net *deposition*, rather than net *erosion*, including even the outer strike point region

[10]: the main chamber walls act as a net source of eroded material which then accumulates everywhere in the divertor. This points to a possible way of avoiding erosion wear of the divertor targets, although it creates its own problems, namely the accumulation of unwanted material (slag) in the divertor which may create dust and debris resulting in disruptions and other operational problems.

(c) Potentially, there is a larger, operationally easier and potentially more flexible window of operation with T_t somewhat greater than $T_t^{\text{sput-thresh}}$. This is possible in principle if there is very strong suppression of the *effective* sputtering rate by prompt, local re-deposition of sputtered material: when the ionization mean free path, mfp, for the sputtered impurity neutral $L_{\text{ioniz}} < 3$–$10\rho_{\text{DT}}$ (where ρ_{DT} is the fuel ion Larmor radius), then the strong E-field and the strong frictional coupling to the fast flow of the fuel ions in the magnetic pre-sheath (MPS) (which is of thickness ~3–$10\rho_{\text{DT}}$ [13]) can promptly return the ionized impurity to the target [14]. In addition, when $L_{\text{ioniz}} < \rho_Z$ (the impurity ion Larmor radius) then before the ionized impurity has completed one gyro-orbit, it will strike the surface again and be deposited [15]. In the appendix it is shown that these prompt removal processes should, in principle, be quite effective at $T_t \lesssim 10\,\text{eV}$ and $n_t \gtrsim 10^{21}\,\text{m}^{-3}$, where $L_{\text{ioniz}} < \rho_{\text{DT}}$ and/or ρ_Z for both W and C.

We next show that achievement of solutions (a) or (b) require roughly the same divertor density n_t as does solution (c).

Fixing the target plasma conditions has the serendipitous benefit that upstream plasma conditions depend very robustly on downstream, i.e. divertor, plasma conditions, see e.g. chapter 12 of [5]. This increases confidence in predictive capability for this approach where the target, i.e. *downstream*, plasma conditions are taken as imposed rather than the *upstream* ones. Furthermore, as shown below, all upstream edge quantities of interest depend more strongly on T_t and n_t than on other quantities, for the most part, which is the reason for placing primary focus in this work on the specification of these two quantities as *input, control* quantities.

Following the extended two-point model, see e.g. section 5.4 in [5], for pressure balance:

$$2n_t(T_{et} + T_{it}) = f_{\text{mom}} n_u (T_{eu} + T_{iu}), \tag{1}$$

where f_{mom} represents the momentum loss due to ion–neutral (i–n) friction, etc; this quantity only becomes significantly different from unity as detachment is closely approached. Here we assume strong collisionality in the divertor, thus $T_{it} = T_{et}$, and weak collisionality upstream in the main part of the SOL. The sparse data set indicates that T_{iu} tends to be higher than T_{eu} and can be a few times T_{eu}, see references in [16]. We define

$$f_{i/e} \equiv 1 + T_{iu}/T_{eu}, \tag{2}$$

a quantity which can be treated empirically, although it is also possible to make simple theoretical estimates for it, see below. It is important to note, however, *that since there are few measurements of T_i in the edge, particularly near the separatrix, the important quantity $f_{i/e}$ is not well known*, unfortunately.

Thus from pressure balance:

$$4n_t T_t = f_{\text{mom}} f_{i/e} n_u T_{eu}. \tag{3}$$

Taking $f_{i/e} = 4$ for simplicity and as a typical value [16], then $n_t \sim f_{\text{mom}} n_u T_{eu}/T_t$. The value of T_{eu} is highly insensitive to all inputs, see below, and we may take $T_{eu} \sim 150\,\text{eV}$ roughly for reactor-like conditions. The value of n_u is more or less closely related to the confined plasma density and it may be difficult to achieve useful confined plasma operation with n_u at the separatrix much less than $\sim 5 \times 10^{19}\,\text{m}^{-3}$, within a factor of 2. For solution (a) above, $T_t^{\text{det}} < T_t < T_t^{\text{sput-thresh}}$, we may take $T_t \sim 3\,\text{eV}$; there is not much i–n momentum loss in such attached plasmas, $f_{\text{mom}} \sim 1$; thus from equation (3) $n_t \gtrsim 2.5 \times 10^{21}\,\text{m}^{-3}$, i.e. a density about the same as for solution (c), even a little higher. For solution (b), T_t is still lower but f_{mom} is also lower, roughly compensating each other, and we again come to approximately the same requirement for n_t, namely that it exceeds $\sim 10^{21}\,\text{m}^{-3}$.

Thus the requirements are two separate ones, namely $n_t \geqslant 10^{21}\,\text{m}^{-3}$ while simultaneously $\sim 2\,\text{eV} < T_t \lesssim 10\,\text{eV}$. It will be shown that this implies that a required *minimum heating power*, $P_{\text{heat}}^{\text{minimum}}$, be achieved corresponding to a specified value of T_t, which for illustration is taken to be 5 eV in the following. Values of $P_{\text{heat}} > P_{\text{heat}}^{\text{minimum}}$ are also satisfactory provided they involve increasing n_t above $10^{21}\,\text{m}^{-3}$ but not increasing T_t above ~10 eV; that is the requirements become the two separate ones, namely that $P_{\text{heat}} \geqslant P_{\text{heat}}^{\text{minimum}}$ while simultaneously $\sim 2\,\text{eV} < T_t \lesssim 10\,\text{eV}$.

Such high plasma densities are also attractive for strong P_{rad}-cooling, fuel and He-ash pumping and for cooling the SOL ions (by equipartition) before they strike the target, see further discussion below. It is fortunate that the divertor conditions required to achieve a solution to the paramount erosion-wear problem of the divertor, are also generally advantageous with regard to a number of other important edge, divertor and PFC issues. It is essential that the deposited power density at the divertor strike points, q_{dep}, should not exceed engineering limitations, which is $q_{\text{dep}}^{\text{maximum}} \sim 10\,\text{MW}\,\text{m}^{-2}$; for $T_e = 5\,\text{eV}$ and $n_e = 10^{21}\,\text{m}^{-3}$, the parallel power flux density $q_\parallel \sim 100\,\text{MW}\,\text{m}^{-2}$ and thus $q_{\text{dep}} = \sin\alpha q_\parallel$ is acceptable provided the angle between $\boldsymbol{B}$ and the divertor surface, α, does not exceed a few degrees which is readily achievable.

While failure to solve the power handling and He-ash removal issues would prevent power reactor operation just as much as failure to solve the net erosion issue would, the former issues will necessarily have been resolved in pre-reactor devices such as ITER, devices which will not necessarily have resolved the net erosion issue. For pre-reactor devices there is the option of achieving successful operation using plasma conditions which would not be consistent with acceptable net erosion rates in a reactor. Because the annual fluence of D/T ions to surfaces will be orders of magnitude greater in power reactors even than in ITER, table 1, power reactors are distinguished by the necessity of solving the net erosion problem which makes it the paramount boundary plasma issue for power reactors. This also establishes the requirements for *reactor-relevant* operation of pre-reactor devices.

In the sheath-limited regime it is expected that $T_{iu} \gg T_{eu}$ due to the nature of the sheath which absorbs the entire ion

population; thus the sheath removes ion power but without cooling the ions, i.e. without acting to reduce the temperature of the ions as they transit through the SOL and sheath, see e.g. section 4.4 of [5]. By contrast the sheath reflects all the low-energy electrons, allowing only the energetic electrons to pass, i.e. the sheath acts as a high-energy pass-filter for the electrons: in order to escape over the sheath barrier the rejected electrons have to collide with other electrons until they are knocked up to high enough energy to escape. Thus the sheath acts not only to remove electron power but to reduce the electron temperature in the SOL as well—an effect not experienced by the ions. From a practical viewpoint this situation is problematic as it can result in high-energy ions—with energies perhaps typical of the top of the pedestal—reaching the solid surfaces, causing strong sputtering. Fortunately, the ions may be cooled through equipartition in the highly collisional divertor plasma—that is assuming n_t is high enough—thus reducing the risk of strong sputtering of the divertor targets. This is another important reason why n_t must be 'high' in a power reactor divertor. It is difficult to make the latter collisional requirement quantitatively precise since the spatial extent within the divertor plasma over which n is high and T is low is quite sensitive to divertor conditions—primarily n_t and T_t. Therefore, independent of the complexity involved, cooling of the ions before they hit the target is also strongly and mainly controlled by the absolute values of n_t and T_t.

In the conduction-limited regime there is a further effect tending to make $T_{iu} \gg T_{eu}$, namely that the Spitzer thermal conductivity of ions is much less than for electrons, see the next section.

Since the neutral pressure in the divertor is closely coupled to the divertor plasma pressure—particularly when $p_t \sim n_t k T_t$ is high [17]—this is a further reason why p_t needs to be high in power reactor divertors, as this considerably aids pumping, including helium-ash removal. It may be noted that for high values of p_t the neutral pressure in the divertor may not be very sensitive to the shape/size of the divertor plasma—nor to the shape of the divertor solid structures; neutral–neutral collisions may be more important than neutral–surface collisions regarding particle transport to pumps [17].

3. Extended two-point modelling to estimate the machine size (R) dependence of upstream plasma conditions, n_{eu} and T_u

Here we address the following question: with n_t and T_t specified as constraints, what is the dependence of the upstream plasma conditions on machine size R? It turns out that the upstream plasma conditions for a *power reactor* are also approximately fixed, independent of R.

Continuing with the extended two-point model, see e.g. section 5.4 of [5]: from power balance:

$$(1 - f_{power}) q_{\parallel} = \gamma k T_t n_t c_{st}, \tag{4}$$

where $q_{\parallel}$ is the total power flux density in the parallel direction upstream, γ is the sheath heat transmission coefficient, see e.g. section 25.5 of [5], c_{st} is the plasma sound speed at the target and $f_{power} q_{\parallel} = P_{vol\ loss}$, the volumetric power loss in the SOL and divertor due to radiation and charge exchange, cx.

Some fraction f_{P_e} of the power entering the SOL to drive $q_{||}$ goes to the electrons, the rest to the ions: $q_{\parallel e} \equiv f_{P_e} q_{\parallel}$. *The value of f_{P_e} is also not well known*, unfortunately.

From parallel electron heat transport:

$$T_{eu} \approx \left(\frac{7 f_{cond} f_{P_e} q_{\parallel} \pi R q}{2 \kappa_{0e}} \right)^{2/7}, \tag{5}$$

see e.g. section 5.4 of [5], where f_{cond} represents the fraction of the parallel electron power transport which is due to conduction, the rest being due to convection; equation (5) assumes $T_{eu}^{7/2} \gg T_{et}^{7/2}$, which is typically the case. Spitzer heat conductivity is also assumed here; this assumption is returned to in section 4. The connection length is assumed to be $L_{conn} = \pi R q$ and κ_{0e} is the Spitzer heat conduction coefficient. Near the separatrix f_{cond} tends towards unity because of the high values of T_e; however, radially further out in the SOL, f_{cond} decreases. The factor 2 in the denominator assumes that the power enters the SOL at the far upstream end; for the essentially opposite assumption that all the power enters uniformly over its length this factor changes to 4, see e.g. section 4.10 of [5]. Therefore the spatial distribution of the power flux across the separatrix into the SOL is not very important.

Thus

$$T_{eu} = \left(\frac{7 \gamma f_{cond} f_{P_e} k T_t n_t c_{st} \pi R q}{2(1 - f_{power}) \kappa_{0e}} \right)^{2/7}, \tag{6}$$

and

$$n_{eu} = 4 n_t T_t / f_{mom} f_{i/e} T_{eu}. \tag{7}$$

Applying similar considerations to the ions one arrives at a similar equation to (6) and thus it is expected for equal power to ions and electrons that, very roughly,

$$\frac{T_{iu}}{T_{eu}} \sim \left(\frac{\kappa_{0e}}{\kappa_{0D^+}} \right)^{2/7} \sim \left(\frac{2000}{60} \right)^{2/7} = 2.72 \sim 3. \tag{8}$$

This assumes that the ions and electrons are not thermally coupled (at least not upstream of the divertor region) and that parallel convection can be neglected. This is therefore only a rough estimate. Although there are a few measurements of T_i in the SOL, those data indicate ratios something on this order [16]. The above values of κ_{0e}, κ_{0D^+} are for pure hydrogenic plasmas; $\kappa_{0e} \propto Z_{eff}^{-1}$, approximately while κ_{0i} has a more complicated dependence on impurity levels but potentially a stronger one [18].

Equation (6) shows that T_{eu} is a very weak function of n_t and T_t, $T_{eu} \propto n_t^{2/7} T_t^{3/7}$, thus it varies little for the range of parameters of interest here. Indeed T_{eu} is weakly dependent on all input quantities. Results are shown in figure 2 for n_{eu} and T_{eu} as functions of R for the example: $\gamma = 7$, $f_{cond} = 1$, $n_t = 10^{21}\ m^{-3}$, DT plasma, $c_{st} = 2.77 \times 10^4\ m\,s^{-1}$, $q = 3$, $f_{power} = 0.5$, $f_{P_e} = 0.5$, $f_{mom} = 1$, $f_{i/e} = 4$, $\kappa_{0e} = 2000$.

On the other hand, n_u is directly proportional to the divertor (plasma) (static) pressure, $p_t \equiv 2 n_t T_t$, approximately, i.e. it is rather strongly dependent on n_t and T_t—more strongly dependent on those quantities than on the other quantities with the exception, it should be noted, of the poorly known $f_{i/e}$.

Finally, we note that with regard to size scaling, both T_{eu} and n_u are weakly dependent on R: $T_{eu} \propto R^{2/7}$, $n_{eu} \propto R^{-2/7}$. For realistic (practical) divertor conditions in any DT tokamak

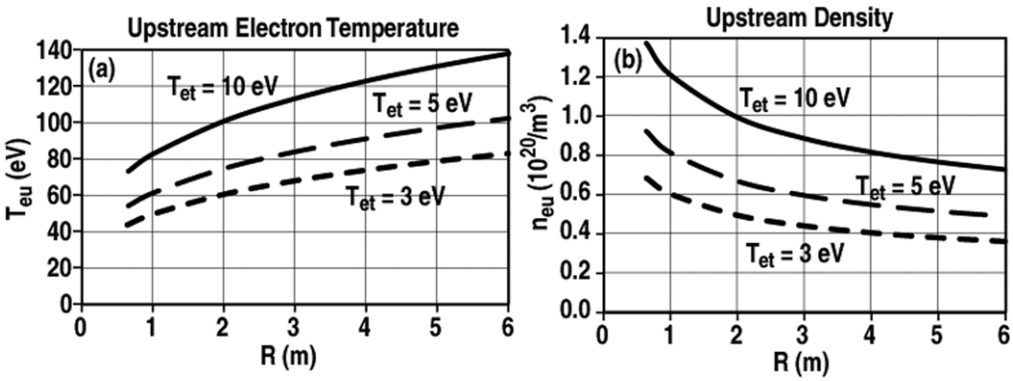

Figure 2. Values of the upstream plasma quantities T_{eu} (left) and n_{eu} (right) as a function of machine size R, for the specific case described in the text: $T_{et} = 10$ eV (solid), 5 eV (long dashed) and 3 eV (short dashed). As noted in the text, the R-dependence is not strong: $T_{eu} \propto R^{2/7}$, $n_{eu} \propto R^{-2/7}$.

power reactor, independent of size, the boundary (separatrix) conditions for the confined plasma will be about the same. Thus the plasma density and temperature, not only at the main interface between plasma and surface (the divertor targets), but also at the interface between the unconfined and confined plasma (the separatrix) are roughly fixed independent of device size for viable DT *power reactors*. (The situation may be different, however, for an *experimental simulator tokamak* used to carry out divertor studies relevant to DT power reactors, see section 7.) It is important to note that the question is not addressed here of whether these separatrix plasma conditions are consistent with acceptable fusion performance in a *power reactor*, i.e. high Q and high central values of $n\tau T$. It is not given that acceptable fusion performance is consistent with viable divertor operation. This critical issue requires assessment outside the scope of the present analysis. It can be seen from figure 2, however, that the upstream separatrix densities required for viable divertor operation turn out, fortunately, to be similar to the densities often associated with good fusion performance, $n_u \sim (5\text{–}10) \times 10^{19}$ m^{-3}.

4. Extended two-point modelling to estimate the power dependence of n_t and T_t

We turn next to the question: what is the minimum power into each leg of the SOL, $P_{SOL}^{one\text{-}leg}$, required to achieve $n_t > 10^{21}$ m^{-3}, simultaneously with T_t in the range 2–10 eV, here specifically $T_t = 5$ eV? Neglecting cross-field power convection:

$$(1 - f_{power}) n_u \chi_\perp k T_{eu} \pi R q / \lambda_{T_{eu}} = f_{P_e} \gamma n_t k T_t c_{st} \lambda_{qt} = (1/4) \gamma n_u k T_{eu} f_{P_e} f_{mom} f_{i/e} c_{st} \lambda_{qt}, \quad (9)$$

$\lambda_{T_{eu}}$ is the radial decay length of T_e at the outside midplane, omp; λ_{qt} is the (total) power decay length at the target (mapped back to the omp, i.e. the effect of magnetic flux expansion is not involved here). Equation (9) neglects convective cross-field power transport; alternatively, the value of $\chi_\perp$ can be considered to be an effective one, including convection. A similar equation to (9) applies to the ions; thus assuming that half the power crosses the separatrix in each of the e and i channels, i.e. $f_{P_e} = 0.5$, then

$$\frac{\lambda_{T_{iu}}}{\lambda_{T_{eu}}} = \frac{T_{iu}}{T_{eu}} \frac{\chi_{\perp i}}{\chi_{\perp e}}. \quad (10)$$

Assuming $\chi_{\perp e} = \chi_{\perp i}$ (*which is also not well known*, unfortunately) then $\lambda_{T_{iu}}/\lambda_{T_{eu}} = T_{iu}/T_{eu} = (f_{i/e} - 1)$ which, as noted, tends to be >1, say 3 or more, although this is also not well known. Thus perhaps $\lambda_{T_{iu}} \sim 3\lambda_{T_{eu}}$ or so.

We may write

$$\lambda_{T_{eu}} = \left[\frac{4(1 - f_{power}) \chi_\perp \pi R q}{\gamma c_{st} f_{P_e} f_{mom} f_{i/e} f_\lambda} \right]^{1/2}, \quad (11)$$

where $f_\lambda \equiv \lambda_{qt}/\lambda_{T_{eu}}$. If all the parallel power were transported all the way to the target by electron heat conduction then it would be expected that $f_\lambda \sim 2/7$, since $q_{\parallel\text{-cond}} \sim T^{7/2}$. There are, however, a number of processes which can be expected to invalidate this assumption such as the contribution of ion parallel power transport. Probably the most important effect, however, is the volumetric power loss in the divertor due to radiation and cx: this is stronger near the separatrix where density is the highest, with the result that the power peak at/near the separatrix gets 'lopped' off, resulting in a broader power distribution at the target than upstream of the divertor. Power leakage across the divertor separatrix into the private flux zone also broadens the power profile in the divertor.

At high values of T_{eu}, kinetic corrections to the Spitzer parallel heat conductivity become important, reducing the effective value of κ_{0e}, see e.g. section 26.2 of [5]; in the extreme of weak collisionality $q_\parallel \propto n_{eu} T_{eu}^{3/2}$, in which case $\lambda_{q_\parallel} = (\lambda_{n_{eu}}^{-1} + 1.5\lambda_{T_{eu}}^{-1})^{-1}$; experimentally $\lambda_{n_{eu}} \sim 2\lambda_{T_{eu}}$ [19] thus $\lambda_{q_\parallel} \sim 0.5\lambda_{T_{eu}}$ would be expected at low collisionality. The collisionality of the SOL electrons can be estimated by the SOL collisional frequency $\nu^*_{SOL_e} \equiv L_{conn}/\lambda_{ee} \approx 10^{-16} n_u L_{conn}/T_{u_e}^2$ for ν (s^{-1}), n (m^{-3}), T (eV) and λ (m), see e.g. equation (4.105) of [5]. It might seem sufficient that $\nu^*_{SOL_e} \gtrsim 1$ for the collisional Spitzer–Harm heat conductivity to hold, however, parallel heat conduction is predominately due to the high-energy electrons in the distribution, ones with $v_e \sim 3\text{–}5 v_{te} \equiv \sqrt{kT_e/m_e}$. Since $\lambda_e \sim v_e^4$ it is actually necessary for $\nu^*_{SOL_e} \gtrsim 100$ for Spitzer–Harm heat conductivity to hold strictly, see e.g. [20] and discussion in section 26.2 of [5]. A detailed analysis [21] shows that Spitzer–Harm is a good approximation for $\nu^*_{SOL_e} \gtrsim 10$ and that flux-limited conduction is a good approximation for $\nu^*_{SOL_e} \lesssim 1$. If $n_u \sim 5 \times 10^{19}$ m^{-3}, $T_{eu} \sim 150$ eV and $L_{conn} \sim 50$ m, then $\nu^*_{SOL_e} \sim 10$ and so we may expect to find the start of a transition to $\lambda_{q_\parallel} \sim 0.5\lambda_{T_{eu}}$ rather than

$\lambda_{q_{||}} \sim \frac{2}{7}\lambda_{T_{eu}}$, just due to this effect alone. It may be noted that it is essential for reactors to avoid the fully flux-limited regime, i.e. very small $\nu^*_{SOL_e}$, which results in small parallel temperature gradients, i.e. the sheath-limited regime, thus high T_t for any significant power level.

From analysis of experimental measurements from a number of tokamaks Whyte [22] has established empirically that $f_\lambda \sim$ unity, with scatter of a factor ~2, which would seem to be very roughly in accordance with the effects just described.

For the same example as above, namely $\gamma = 7$, $T_t = 10\,\text{eV}$, DT plasma, $c_{st} = 2.77 \times 10^4\,\text{m s}^{-1}$, $q = 3$, $f_{power} = 0.5$, $f_{mom} = 1$, $f_{i/e} = 4$, $f_{P_e} = 0.5$, then equation (11) gives

$$\lambda_{T_{eu}}(\text{m}) = 0.0070(R\chi_\perp/f_\lambda)^{1/2}, \tag{12}$$

for R(m) and $\chi_\perp$ ($\text{m}^2\,\text{s}^{-1}$). The power entering one leg of the SOL, $P_{SOL}^{one\text{-}leg}$ (MW), is related to the parallel power flux density at the upstream of the divertor leg, $q_{||}$ (MW m^{-2}):

$$q_{||} = \frac{P_{SOL}^{one\text{-}leg}}{2\pi R\lambda_{qt} b_u}, \tag{13}$$

where $b_u \equiv (B_\theta/B_\phi)_u$ (strictly $\sin[\tan^{-1}(b_u)]$ should be used in equation (13), rather than b_u), giving

$$\frac{P_{SOL}^{one\text{-}leg}}{R} = 2\pi b_u n_t k T_t \left[\frac{\gamma c_{st}\lambda_{qt}}{(1 - f_{power})}\right]. \tag{14}$$

While equation (14) gives the value of $P_{SOL}^{one\text{-}leg}$ required for any general, specified values of n_t and T_t, the point here is that it also gives the *minimum* value $P_{SOL}^{one\text{-}leg}$ for values of n_t greater than some specified value, here $10^{21}\,\text{m}^{-3}$, for a specified value of T_t, here taken to be 5 eV for illustration. Thus for the lowest value of divertor temperature of interest here, $T_t \sim 2\,\text{eV}$, the required minimum value of $P_{SOL}^{one\text{-}leg}$ will be somewhat lower.

Using equation (11) and the definition of f_λ to estimate λ_{qt} gives

$$\frac{P_{SOL}^{one\text{-}leg}}{R^{3/2}} = 2\pi b_u n_t k T_t \left[\frac{4\gamma\chi_\perp \pi q c_{st} f_\lambda}{f_{P_e} f_{mom} f_{i/e}(1 - f_{power})}\right]^{1/2}. \tag{15}$$

One may note that, again, the scaled quantity is linearly related to the divertor pressure p_t, approximately (as is $q_{||}$ also) and that this dependence is stronger than (almost all of) the other dependences.

Next, with regard to size scaling we will consider four possibilities here for evaluating λ_{qt}.

4.1. *Case of* λ_{qt} = constant *[23]*

It was argued by Goldston, [23], on the basis of our current limited understanding and data, that the approximation $\lambda_{qt} \sim$ constant, independent of machine size, power, etc, is as reliable as a more complex analysis; see figure 5 in [24], which may be interpreted to indicate $\lambda_{qt} \sim 8\,\text{mm}$, constant. In this case, one does not use equations (11), (12) or (15) but the more basic equation (14) which with $\lambda_{qt} \sim 8\,\text{mm}$ gives

$$\left.\frac{P_{SOL}^{one\text{-}leg}}{R}\right|_{\lambda_{qt}=\text{constant}} = (0.008)2\pi b_u n_t k T_t \left[\frac{\gamma c_{st}}{(1 - f_{power})}\right]. \tag{16}$$

Example: DT plasma, $b_u = 0.3$, $n_t = 10^{21}\,\text{m}^{-3}$, $\gamma = 7$, $f_{power} = 0.5$, gives for $T_t = 5\,\text{eV}$:

$$\left.\frac{P_{SOL}^{one\text{-}leg}}{R}\right|_{\lambda_{qt}=\text{constant}} = 3.31(\text{MW m}^{-1}). \tag{17}$$

Also

$$\left.\frac{P_{SOL}^{one\text{-}leg}}{R}\right|_{\lambda_{qt}=\text{constant}} \propto n_t T_t^{3/2}. \tag{18}$$

4.2. *Case of* $\chi_\perp$ = constant *with an empirical* $f_\lambda \equiv \lambda_{qt}/\lambda_{T_{eu}}$ = constant *[22]*

For the simple but arbitrary assumption of $\chi_\perp =$ constant, together with Whyte's empirical $f_\lambda \equiv \lambda_{qt}/\lambda_{T_{eu}} =$ constant [22], equation (15) gives $P_{SOL}^{one\text{-}leg} \propto R^{3/2}$:

$$\left.\frac{P_{SOL}^{one\text{-}leg}}{R^{3/2}}\right|_{f_\lambda=\text{constant}} = 2\pi b_u n_t k T_t \times \left[\frac{4\gamma\chi_\perp\pi q c_{st} f_\lambda}{f_{P_e} f_{mom} f_{i/e}(1 - f_{power})}\right]^{1/2}. \tag{19}$$

Example: DT plasma, $q = 3$, $b_u = 0.3$, $n_t = 10^{21}\,\text{m}^{-3}$, $\gamma = 7$, $f_{mom} = 1$, $f_{power} = 0.5$, $f_{P_e} = 0.5$, $f_{i/e} = 4$, $\chi_\perp = 1\,\text{m}^2\,\text{s}^{-1}$, $f_\lambda = 1$, then for $T_t = 5\,\text{eV}$:

$$\left.\frac{P_{SOL}^{one\text{-}leg}}{R^{3/2}}\right|_{f_\lambda=\text{constant}} = 2.88(\text{MW m}^{-3/2}). \tag{20}$$

Also,

$$\left.\frac{P_{SOL}^{one\text{-}leg}}{R^{3/2}}\right|_{f_\lambda=\text{constant}} \propto n_t T_t^{5/4}\chi_\perp^{1/2} f_\lambda^{1/2}. \tag{21}$$

4.3. *Case of an empirical* $\lambda_{eu} = 0.003R$ *[19] combined with an empirical* $f_\lambda \equiv \lambda_{qt}/\lambda_{T_{eu}}$ = constant *[22]*

Kallenbach *et al* [19] reported that $\lambda_{eu} \propto R$ which implies that $\chi_\perp \propto R$, equation (12). In this case $P_{SOL}^{one\text{-}leg} \propto R^2$. For JET ($R = 3\,\text{m}$) Kallenbach reports that $\lambda_{eu} =$ 7–10 mm; Kirnev *et al* [25] report $\lambda_{qt} \sim 5.5\,\text{mm}$ as a representative JET value; thus as noted by Whyte, λ_{qt} and $\lambda_{T_{eu}}$ are roughly comparable.

Setting Kallenbach's empirical $\lambda_{T_{eu}}(\text{m}) \approx 0.003R(\text{m})$ equal to $\lambda_{T_{eu}}(\text{m}) = 0.0070(R\chi_\perp/f_\lambda)^{1/2}$, equation (12), gives $\chi_\perp^{Kallenbach} = 0.18R$, for $f_\lambda = 1$ and so for $R = 1$, 2.5 and 6 m, $\chi_\perp^{Kallenbach} = 0.18$, 0.45 and $1.1\,\text{m}^2\,\text{s}^{-1}$.

Using Kallenbach's $\lambda_{T_{eu}} = 0.003R$, rather than specifying $\chi_\perp$ as required in case 4.2, then gives

$$\left.\frac{P_{SOL}^{one\text{-}leg}}{R^2}\right|_{\lambda_{qt}\propto R} = (0.003)2\pi b_u n_t k T_t \left[\frac{\gamma c_{st} f_\lambda}{(1 - f_{power})}\right]. \tag{22}$$

Example: DT plasma, $b_u = 0.3$, $n_t = 10^{21}\,\text{m}^{-3}$, $\gamma = 7$, $f_{power} = 0.5$, $f_\lambda = 1$ gives for $T_t = 5\,\text{eV}$:

$$\left.\frac{P_{SOL}^{one\text{-}leg}}{R^2}\right|_{\lambda_{qt}\propto R} = 1.24(\text{MW m}^{-2}), \tag{23}$$

and

$$\left.\frac{P_{SOL}^{one\text{-}leg}}{R^2}\right|_{\lambda_{qt}\propto R} \propto n_t T_t^{3/2} f_\lambda. \tag{24}$$

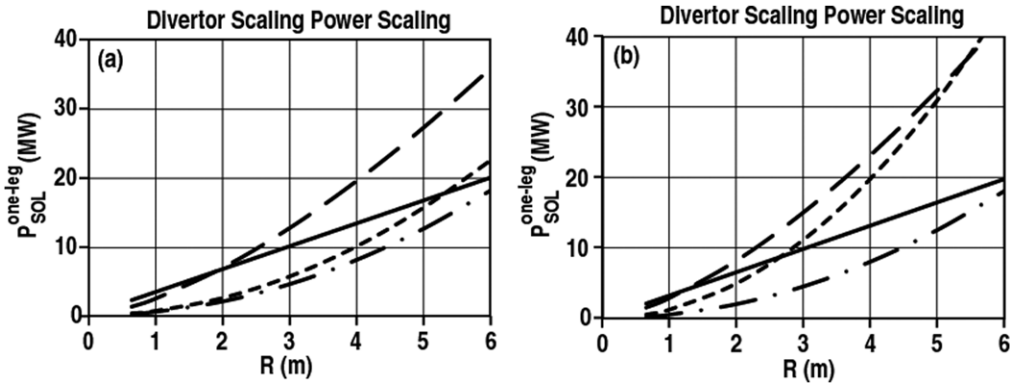

Figure 3. Effect of machine size, R, on the required power into one leg of the SOL to achieve $n_t = 10^{21}\,m^{-3}$ and $T_t = 5\,eV$, for the four different scaling relations. 'λ_{qt} = constant' (solid), 'f_λ = constant' (long dashed), '$\lambda_{qt} \propto R$' (short dashed), 'JET' (dotted–dashed). Also assumed: DT plasma, $b_u = 0.3$, $B_\phi = 5\,T$, $q_{95} = 3$, $f_{power} = 0.5$, $f_{P_e} = 0.5$; also $n_{ue} = 5 \times 10^{19}\,m^{-3}$ for 'JET' scaling and $\lambda_{qt} = 8\,mm$ for 'λ_{qt} = constant' scaling. Two cases are shown: (*a*) (left) $\chi_\perp = 1\,m^2\,s^{-1}$, $f_{mom} = 1$, $f_{i/e} = 4$, $f_\lambda = 0.5$; (*b*) (right) $\chi_\perp = 0.25\,m^2\,s^{-1}$, $f_{mom} = 0.7$, $f_{i/e} = 2$, $f_\lambda = 1$. Assuming two equal divertor legs and that 50% of the total heating power P_{heat} (external plus *α-heating*) is radiated in the main plasma, this plot gives P_{heat} if the vertical scale is multiplied by 4.

4.4. Case of JET scaling [25]

Kirnev *et al* [25] report the following scaling for ELM-averaged JET discharges:

$$\lambda_{qt}^{JET} = 0.0055 \left(\frac{B_\phi}{2.5}\right)^{-1} \left(\frac{P_{SOL}^{one\text{-}leg}}{5}\right)^{-0.5} \left(\frac{n_{ue}}{2}\right)^{0.25} \times \left(\frac{q_{95}}{3}\right) \left(\frac{R}{3}\right)^2, \quad (25)$$

for λ(m), B(T), P(MW), $n(10^{19}\,m^{-3})$ and R(m). In order to separate out the factors of $P_{SOL}^{one\text{-}leg}$ and R we define

$$\hat{\lambda}_{qt}^{JET} \equiv 0.0055 \left(\frac{B_\phi}{2.5}\right)^{-1} \left(\frac{1}{5 \times 10^6}\right)^{-0.5} \left(\frac{n_{ue}}{2}\right)^{0.25} \times \left(\frac{q_{95}}{3}\right) \left(\frac{1}{3}\right)^2. \quad (26)$$

Inserting λ_{qt}^{JET} into equation (14) we obtain

$$\left.\frac{P_{SOL}^{one\text{-}leg}}{R^2}\right|_{JET} = \left[\frac{2\pi b_u n_t k T_t \gamma c_{st} \hat{\lambda}_{qt}^{JET}}{(1 - f_{power})}\right]^{2/3}. \quad (27)$$

Example: DT plasma, $B_\phi = 5\,T$, $n_{ue} = 5 \times 10^{19}\,m^{-3}$, $q_{95} = 3$, $b_u = 0.3$, $n_t = 10^{21}\,m^{-3}$, $\gamma = 7$, $f_{power} = 0.5$ and $T_t = 5\,eV$:

$$\left.\frac{P_{SOL}^{one\text{-}leg}}{R^2}\right|_{JET} = 0.501\ (MW\,m^{-2}). \quad (28)$$

Also,

$$\left.\frac{P_{SOL}^{one\text{-}leg}}{R^2}\right|_{JET} \propto n_t^{2/3} T_t B^{-2/3}. \quad (29)$$

Results for the four power scalings are shown in figure 3 for some examples of the controlling parameters.

As can be seen from these figures there is not a large difference among the four power scalings; for the most part about a factor of order ~2 difference for the required heating power for a significant range of R. More specifically, for the four scalings and for integer values of R from 1 to 6 m the normalized standard deviation (normalized by the average value), then averaged for the 6 values of R, gave 0.49 (0.48) for figure 3(*a*) (figure 3(*b*)), i.e. 'a factor of ~2 difference'. Such differences are less than the uncertainties involved in the simple modelling and for the assumed values of parameters such as $\chi_\perp$, $f_{i/e}$ and f_λ. There are other plausible choices for the control parameters which can cause larger (also smaller) differences among the four power scalings; however, there is evidently a degree of robustness to the situation indicated by figure 3, namely a tendency for there not to be a great difference among the four power scalings, a tendency which can be made clear by varying the control parameters over plausible ranges. It is perhaps not surprising that the four power scalings tend to converge since they are all essentially empirically based. Even the values used for $\chi_\perp^{SOL}$ really come from experiments, where it has been found from many exercises in matching midplane radial T-profiles by edge codes that values of order $1\,m^2\,s^{-1}$ are required to get agreement. Greater differences might be expected if different physics assumptions had been used in first-principles theories for the power scalings, but the only theoretical component of the analysis used here is the two-point modelling, which is no more than the fundamental conservation equations in a simple form.

This robustness is very valuable since it means that coming at the problem in different ways leads to roughly the same conclusion about the amount of power required to achieve the necessary divertor conditions. The fact that the different scalings are all heavily empirical is also reassuring.

Assuming two equal divertor legs and that 50% of the total heating power P_{heat} (external plus *α-heating*) is radiated in the main plasma, then figure 3 gives P_{heat} if the vertical scale is multiplied by 4. Thus to achieve $n_t > 10^{21}\,m^{-3}$ in ITER, for example, where $R = 6\,m$, one requires a minimum of $P_{heat} \sim$ 80–160 MW for $T_t = 5\,eV$ and roughly half (double) the power for $T_t = 2(10)\,eV$ (only roughly since the relation between and n_e and T_e profiles at the target may change and this is not dealt with by the simple two-point modelling). At $Q = 10$, the sum of external and alpha heating in ITER will be ~150 MW. Therefore, it would appear that ITER will access this reactor-relevant regime. Since the value of n_t has to satisfy a *minimum* constraint there is some flexibility regarding the

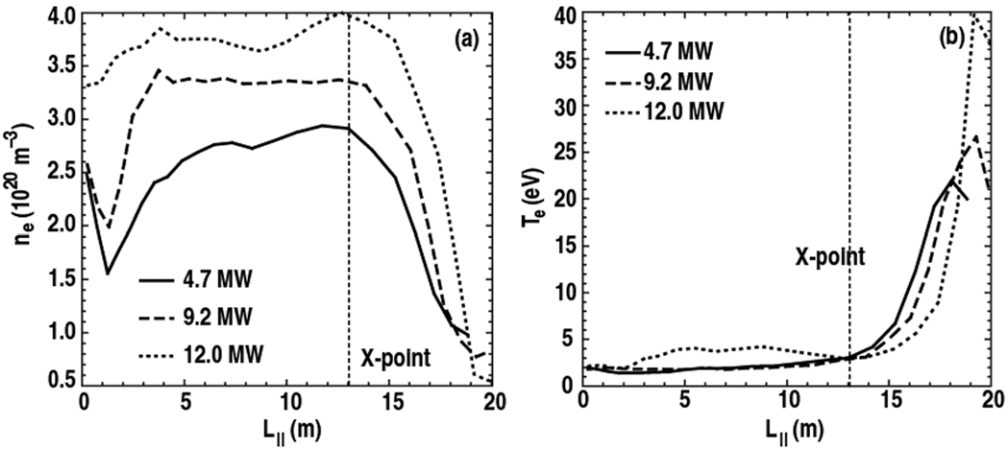

Figure 4. The DTS-measured plasma density $n_e(s_{||})$ (left) and $T_e(s_{||})$ (right) for high-density, high-power detached DIII-D discharges.

associated value of n_u, which may be important for achieving the desired core performance simultaneously with reactor-relevant divertor operation.

The four power scalings have a roughly similar dependence on volumetric power loss in the SOL/divertor, namely $P_{SOL}^{one\text{-}leg} \propto (1 - f_{power})^n$, $n = -1$ to $-1/2$. The *total* volumetric power loss includes loss in the confined plasma. $P_{rad}^{total} \sim 75\% P_{heat}$ is representative of operating conditions that are somewhat away from the density limit [4], with roughly half of P_{rad}^{total} occurring in the confined plasma and half outside the separatrix, i.e. $f_{power} \sim 0.5$, typically. As divertor conditions approach full detachment, f_{power} increases, increasing $P_{SOL}^{one\text{-}leg}$ roughly by the same amount for the four power scalings. As $f_{power} \to 1$, $P_{SOL}^{one\text{-}leg} \to \infty$ and the foregoing simple analysis becomes only qualitative.

5. Present edge diagnostic capability and the problem of testing edge model predictions for high-density, low-temperature divertor operation

It is important to establish whether any of the power scalings are supported by experimental measurements in present devices for the very high-density, low-temperature divertor regime that is of interest here: most of the empirical basis for the four power scalings involved much less dense and hotter divertor conditions.

As already noted, unfortunately a number of key quantities needed to test the previously described models are not measured at present in any tokamak:

(a) f_{P_e}, the fraction of the power entering the SOL in the electron channel is not measured.
(b) $T_{D_u^+}$ at the upstream separatrix is rarely measured.
(c) In principle f_{mom} could be deduced from $f_{mom} = 4n_t T_{et}/f_{i/e} n_u T_{eu}$ since n_t, T_{et}, n_u, and T_{eu} can be directly measured; however, since $T_{D_u^+}$ is not measured, $f_{i/e}$ is not known which prevents the deduction of f_{mom}.
(d) f_{cond}, the fraction of the parallel power flux density carried by conduction is not measured.

Fortunately the divertor Thomson system, DTS, in DIII-D [26] makes it (only just) possible to either directly measure or deduce all of the above quantities, thus making it possible, in principle, to test the simple edge-model predictions described above. DTS makes it possible to measure n_e and T_e throughout the divertor, extending somewhat upstream beyond the X-point in the outer SOL where the parallel gradients tend to become small. At a location still further 'upstream' a second Thomson system provides radial profiles of n_e and T_e. Thus, effectively, $n_e(s_{||})$ and $T_e(s_{||})$ can be measured in 2D completeness for the outer divertor and SOL of DIII-D (here $s_{||}$ is measured along the field line starting from the outer target, for each radial location). From such data sets, e.g. those in [27, 28], it is then possible to infer with fair reliability a number of important quantities of the outer SOL:

(a) the location, defined to be $s_{||}^*$, where $q_{||e}$ changes from conduction (upstream of $s_{||}^*$) to convection (below),
(b) the location where the flow speed reaches $M_{||} \sim 1$, which is about the same location as $s_{||}^*$ [27, 28],
(c) the location where frictional momentum loss starts to occur: the loss of static (measured) electron pressure by the point where $M_{||}$ reaches $\sim$ unity is only a factor of 2 if there is no frictional momentum loss upstream of the sonic transition. Thus from measured electron pressure profiles, $p_e(s_{||})$, the location where f_{mom} is still $\sim$ unity can be identified. For the DIII-D shots [27, 28] this location was also at $s_{||}^*$, approximately, which for field lines near the separatrix was at $s_{||}^* \sim 17$ m (just upstream of the divertor entrance at $s_{||}^* \sim 13$ m, figure 4).

It is therefore appropriate to choose location $s_{||}^*$ to be the virtual target location, rather than using the actual target location since then:

(a) it can reasonably be concluded that $f_{cond} \sim 1$ above this point,
(b) f_{P_e} can be deduced from equation (6) since all the other quantities are known or measured (f_{power} is deduced from 2D bolometric measurements),
(c) It can reasonably be concluded that $f_{mom} \sim 1$ above this point and thus $f_{i/e}$ can be deduced from $f_{i/e} = 4n_t T_{et}/n_u T_{eu}$.

If the divertor condition of interest here had been low-density, high-temperature, i.e. well-attached, divertor operation, then an abundance of experimental data would be available, from many tokamaks, where two of these 'unknown'

factors would, in fact, be known: namely it could be safely assumed that $f_{\rm cond} \sim 1$ and $f_{\rm mom} \sim 1$ and then the procedure just indicated for deducing f_{P_e} and $f_{i/e}$ could be employed. However, as pointed out above the divertor condition that we need to test here is high density and low temperature, and so if the only location where divertor conditions are measured is at the target—which is the usual situation—then there is insufficient experimental input to test the above modelling.

6. Testing the four power scalings using data from a set of high-density, high-power DIII-D discharges

The discharges used here are ones that have been documented in DIII-D radiative divertor studies [27, 28] where the focus was on the strong volumetric losses occurring within the divertor, rather on the relation between the upstream (outer midplane) and the entrance to the divertor, i.e. the virtual target, which is the focus here. These discharges are of special interest here because they had divertor conditions approaching the $n_t \sim 10^{21}\,{\rm m}^{-3}$, $T_t \sim 5\,{\rm eV}$ regime, and they were also particularly well diagnosed, specifically employing the divertor Thomson scattering system in DIII-D [26]. Figure 4 shows the DTS-measured $n_e(s_{||})$ and $T_e(s_{||})$ profiles for a number of high-density, high-power discharges; these profiles are averaged over magnetic flux surfaces $\psi = 1.0$–1.004, which is ~2 mm at the outer midplane. The discharges were in H-mode, lower single null, with plasma current 1.4 MA, $B_\phi = 2\,{\rm T}$, safety factor $q_{95} \sim 3.9$ and a neutral beam injected power of 4–12 MW. The virtual target location was taken to be where $T_e = 5\,{\rm eV}$, which as noted was at $s_\parallel \sim 17\,{\rm m}$, i.e. just upstream of the X-point, i.e. the divertor entrance. The DTS measurements thus provide the values for n_t and $T_t(=5\,{\rm eV})$ at the virtual target; the precise radial location is not critical as long as it is approximately one half a power width from the separatrix; thus identifying the precise location of the separatrix is also not critical.

Following the analysis procedure in [27, 28], the SOL was treated as a 1D plasma as a function of $s_{||}$. The plasma radiation, $\varepsilon(s_{||})$, was measured by two poloidally separated 24-channel bolometer arrays [29] whose view chords are shown in figure 2 of [28]. The signals from these two arrays were inverted to produce a 2D radiation profile, also shown in figure 2 of [28]. This profile was integrated radially through the divertor SOL and with the assumption of toroidal symmetry produced a 1D profile of radiation, $\varepsilon_{\rm SOL}(s_{||})$. The total power, $Q_{\rm tot}(s_{||})$, flowing in this 1D divertor approximation was calculated by starting with the divertor target heat flux measured by an IR camera and integrating the 1D radiation profile. Contributions from plasma radiation and edge-localized modes (ELMs) were subtracted from the target heat flux. From $Q_{\rm tot}(s_{||})$ the values of $P_{\rm SOL}^{\rm one\text{-}leg}$ and $f_{\rm power}$ were obtained. The parallel heat flux density, $q_{\rm tot}(s_{||})$, figure 5 in [28], was obtained by dividing by the cross-sectional area of the SOL perpendicular to the magnetic field. The SOL area normal to the magnetic field lines is determined by the heat flux width at the divertor plate, in conjunction with magnetic equilibrium measurements, and remains constant through the divertor, assuming constant SOL magnetic flux. Values of $q_{\rm tot}(s^*_{||})$ are given in table 2. It should be noted that the values of λ_{qt} that were measured by IR, see figure 3 of [28], cannot be directly used to test the four cases of section 4 since the divertor was strongly detached and here the primary interest is in dense, cold, but not detached, divertor conditions.

Table 2. Measured and deduced parameters for three high-density, high-power DIII-D discharges. The values of $T_{C^{6+}u}$ were measured by CER, cx spectroscopy. Also used: $R = 1.65\,{\rm m}$, $q = 3.9$, $B_\theta/B_\phi = 0.27$, $I_p = 1.4\,{\rm MA}$, $B_\phi = 2\,{\rm T}$.

Case. $P_{\rm heat}$ (MW)	4.7	9.2	12
n_t (at 5 eV) ($10^{20}\,{\rm m}^{-3}$)	2.6	3.0	3.3
$q_{\rm tot}(s^*_\parallel)$ i.e. at 5 eV (MW m^{-2})	23.5	36	56
$\gamma_{\rm eff}$	5.16	6.85	9.69
$n_{\rm eu}$ ($10^{20}\,{\rm m}^{-3}$)	0.21	0.25	0.35
$T_{\rm eu}$ (eV)	40	50	75
$P_{\rm SOL}^{\rm outer\text{-}leg}$(MW)	1.27	1.9	2.75
$f_{\rm power}$	0.43	0.63	0.56
$f_{\rm mom}$	1	1	1
$f_{\rm cond}$	1	1	1
$f_{i/e}$	6.19	4.8	2.51
T_{D^+u} ($T_{C^{6+}u}$) (eV)	200 (160)	190 (160)	113 (130)
f_{P_e}	0.16	0.2	0.82

Table 3. Measured and scaling values of $P_{\rm SOL}^{\rm outer\text{-}leg}$. Assumed here: $\lambda_{qt} = 8\,{\rm mm}$, $\chi_\perp = 1[{\rm m}^2\,{\rm s}^{-1}]$ and $f_\lambda = 1$.

Case. $P_{\rm heat}$ (MW)	4.7	9.2	12
Measured $P_{\rm SOL}^{\rm outer\text{-}leg}$ (MW)	1.27	1.9	2.75
Goldston $P_{\rm SOL}^{\rm outer\text{-}leg}$ (MW)	0.89	2.3	2.9
Whyte $P_{\rm SOL}^{\rm outer\text{-}leg}$ (MW)	2.3	4.1	3.2
Kallenbach–Whyte $P_{\rm SOL}^{\rm outer\text{-}leg}$ (MW)	0.55	1.4	1.8
JET $P_{\rm SOL}^{\rm outer\text{-}leg}$ (MW)	0.77	1.5	1.8

The values of $n_{\rm eu}$ and $T_{\rm eu}$ were measured by a second Thomson scattering system located near the outer midplane; as with n_t and T_t, the precise radial location is not critical. For these discharges $Z_{\rm eff}^{\rm main}$ was ~1.3; there were no measurements of $Z_{\rm eff}^{\rm SOL}$ but assuming that $Z_{\rm eff}^{\rm SOL} > Z_{\rm eff}^{\rm main}$, then $Z_{\rm eff}^{\rm SOL} = 2$ was estimated and used to give $\kappa_{0e} = 1000$. The values of $f_{i/e}$ and f_{P_e} were deduced by the procedure discussed in section 5. The values of the parameters are tabulated in table 2. One difference between an actual divertor target and a virtual target is the value to be assigned for the sheath heat transmission coefficient γ, or equivalent; at an actual target $\gamma \sim 7$, for $T_{et} = T_{it}$, where ~3 of the 7 is due to the electron-repelling sheath that forms in front of an actual target surface; no sheath need exist at a mid-flow sonic transition point and there one expects $\gamma \sim 2{+}2.5(T_{it}/T_{et})$, see e.g. section 25.5 of [5]. There were no measurements of T_{it} at the virtual target; however, the effective heat transmission coefficient, $\gamma_{\rm eff}$, can be calculated from

$$q_{\rm tot}(s^*_\parallel) = \gamma_{\rm eff} k T_{et} n_t c_{st}. \qquad (30)$$

The values of $\gamma_{\rm eff}$, table 2, exceed 4.5 indicating $T_{it} > T_{et}$. Inserting these parameters into the expressions for the four power scalings in section 4 then gives the results shown in table 3.

From table 3 it is clear that all four scalings agree with the measured values of $P_{\rm SOL}^{\rm outer\text{-}leg}$, for the most part to within a factor of order ~2 for the 3 discharges analysed, which is well within the combined uncertainties of the scalings and

Table 4. Changes required to the values of single key parameters for each of the scalings in order to bring them into exact agreement with the measured $P_{\rm SOL}^{\rm outer\text{-}leg}$. The values in brackets are the ones used in table 3.

Case. $P_{\rm heat}$ (MW)	4.7	9.2	12
Goldston Required value of λ_{qt} (mm). (8)	11	6.7	7.7
Whyte Required value of $\chi_\perp$ ($m^2\,s^{-1}$). (1)	0.32	0.22	0.73
Kallenbach–Whyte Required value of f_λ. (1)	2.3	1.35	1.56
JET Required multiplier of $\hat{\lambda}_{qt}^{\rm JET}$ (1)	2.1	1.5	2.1

the experimental measurements. From this we arrive at two important conclusions:

(a) Even though the four power scalings are based largely on experimental results for divertors that are significantly less dense and typically hotter than is of interest here, they have been shown to also agree to within experimental uncertainties with well-diagnosed DIII-D discharges which had divertor conditions close to those of interest here.

(b) In light of the earlier finding of relative insensitivity to the choice of power-scaling law, figure 3, it is perhaps not surprising that all four scalings agree with the measured values of $P_{\rm SOL}^{\rm outer\text{-}leg}$. Since the combined uncertainties are at least a factor of 2 it is not possible to discriminate amongst the four scalings on the basis of this initial test. However, this study does indicate what power is needed to achieve the required divertor conditions in future devices, for both reactor and simulator tokamaks. As a further indication of how close each of the scalings is to matching measurement, in table 4 the values are given for the changes required to a single key assumption used in table 3 for each of the scalings in order to bring the scaled and measured values of $P_{\rm SOL}^{\rm outer\text{-}leg}$ into exact agreement. It is apparent that the required changes are small and plausible.

7. Simulating reactor-relevant conditions in experimental simulator tokamaks

It is important to be able, if possible, to study the important edge and divertor processes that will occur in a DT fusion reactor in experimental devices which are smaller, or at least less expensive. As argued here, section 3, perhaps the paramount practical issue for DT reactors is the achievement of a very large reduction of the rate of net erosion compared with present tokamak experience. It is therefore particularly important to be able to study the processes involved in prompt, local deposition, see the appendix, in an *experimental simulator tokamak*. Can this be done in a scaled way? That is, without requiring replicating the absolute values of $n_{\rm t} \sim 10^{21}\,{\rm m}^{-3}$ and $T_{\rm t} \sim 5\,{\rm eV}$ required in a *power reactor*?

It is recognized [1, 2] that the plasma temperature at the divertor target, $T_{\rm t}$, cannot be scaled but must be matched absolutely, since so many important divertor processes depend on the (absolute) plasma temperature. Turning to the target density $n_{\rm t}$, as discussed in the appendix, the achievement of strong suppression of net erosion by prompt, local deposition of target sputtered particles requires that $L_{\rm ioniz} < \rho_{\rm DT}, \rho_z$. Since $L_{\rm ioniz}/\rho_{\rm DT}, \rho_z \propto (B/n_{\rm t})$ there exists the possibility of reducing B and $n_{\rm t}$ together in an experimental simulator tokamak, that is the target density can be scaled, at least for carrying out studies specifically on prompt, local deposition. If it is wanted to simultaneously, i.e. for the same operating conditions, study the other important edge/divertor processes, such as divertor pumping and highly radiating divertor properties, then since these different processes have different scaling relations, it would probably be necessary to replicate the actual reactor values of $n_{\rm t}$ and $T_{\rm t}$. It should be possible, however, to study these other edge/divertor processes individually using appropriate specific scalings.

If an experimental simulator tokamak uses reduced magnetic field together with reduced $n_{\rm t}$ (say $2 \times 10^{20}\,{\rm m}^{-3}$), this will reduce the required $P_{\rm heat}$ by 5× relative to that in a reactor (say $n_{\rm t} = 10^{21}\,{\rm m}^{-3}$) of the same size and having the same $T_{\rm t}$, say 5 eV. Reducing $n_{\rm t}$ by 5× while keeping $T_{\rm t}$ fixed will require the use of a 5 × reduced value of $n_{\rm u}$, see equations (6) and (7), which could degrade the fusion performance of the confined plasma, depending on the operating regime. Degraded fusion performance may not be acceptable, even regarding the achievement of the values of $n_{\rm t}$ and $T_{\rm t}$ required for reactor-relevant divertor studies, since the alpha heating could be needed to provide part of the required $P_{\rm heat}$. In that situation it would not be possible to use reduced field and density in the simulator. There would remain the possibility of cost savings by using a smaller machine (R), which also requires smaller $P_{\rm heat}$ for a given $n_{\rm t}$ and $T_{\rm t}$, figure 3, provided the smaller value of required $P_{\rm heat}$ could be achieved in the smaller device.

8. Discussion and conclusions

By way of summary we now return to the four questions posed at the start of section 1, distinguishing between the requirements of *power reactors* and of *experimental simulator tokamaks* used to study critical boundary-related issues relevant to power reactors.

The objective of magnetic fusion is to create a 'star in a bottle'. It seems intuitively obvious that the most challenging practical aspect of this undertaking will be avoiding the destruction of the bottle by the star. Even rough quantitative estimates of the rate of erosion wear of the divertor targets confirm this and indicate that this issue may be the paramount boundary-related one requiring solution. A number of potential solutions can be envisaged but as argued here, they all require achievement of approximately the same plasma conditions in the divertor of a *power reactor*, namely $T_{\rm et} \lesssim 5\,{\rm eV}$ and $n_{\rm et} \gtrsim 10^{21}\,{\rm m}^{-3}$.

It is shown here that these almost fixed divertor plasma requirements in turn imply almost fixed 'upstream' plasma conditions, i.e. at the separatrix at the outer midplane, namely $T_{\rm eu} \sim$ 100–150 eV and $n_{\rm eu} >$ (0.5–1) $\times 10^{20}\,{\rm m}^{-3}$, almost independent of tokamak *power reactor* size and other system parameters.

The heating power required to achieve these boundary plasma conditions for *power reactors* are estimated using four empirical power scalings that have been proposed recently. Although they give different predictions for how the required power varies with R—namely as R, $R^{1.5}$ and R^2—the absolute magnitude of the required power, for a given device size, does not vary much, $\lesssim$ a factor of 2, over a significant range of R,

over the four power scalings. This convergence is probably due to the fact that each of the power scalings is heavily empirical and they are in some sense just different ways of treating the same input information. In any event, this close agreement gives some confidence in our ability to project the heating requirements for current or future devices of specified size, whether power reactors or experimental simulator tokamaks.

The four power scalings, while empirical, are largely based on measurements made in tokamaks that did not have divertor plasma conditions in the $T_{et} \sim 5$ eV, $n_{et} \sim 10^{21}$ m^{-3} range. It is therefore not clear that all or any of the four is actually valid for future devices operating under these conditions. In order to test the four scalings, comparisons were made with measured conditions in a set of high-power, high-density DIII-D discharges which had divertor plasma conditions approaching the above. Again it was found that all four power scalings matched the measured power into the outer SOL to within a factor of ~2, which was well within the combined uncertainties of the measurements and the scalings.

It is therefore concluded, tentatively, based on this initial test on a single tokamak, that each of the power scalings can provide a reliable basis for projecting the heating power required for future fusion power devices and for experimental simulator tokamaks to study reactor-relevant divertor processes. Further comparisons, including ones involving tokamaks of different sizes, will be required to substantiate this conclusion.

It is desirable to be able to study reactor-relevant boundary processes in *experimental simulator tokamaks* of reduced size or at least reduced cost. In order to study the paramount boundary issue of erosion wear, a trade-off can be made between magnetic field strength and divertor density, possibly permitting some cost savings; however, the divertor plasma temperature needs to be matched absolutely since so many critical processes depend on it—indeed this quantity largely defines the very regime in which the boundary plasma operates. Fortunately, the achievement of other critical boundary objectives, such as strong helium pumping and high radiative fractions, benefit in large part by operation under this divertor condition. It is likely that there are also individual scaling for these other processes that will permit trade-offs and cost savings when each of these processes is studied individually. To study them all simultaneously in the same *experimental simulator tokamak*, however, may require $T_{et} \sim 5$ eV and $n_{et} \sim 10^{21}$ m^{-3} in the simulator since each of the processes may have incompatible scalings. It may also not be possible to operate the simulator at reduced values of n_{et} since lower values correspond to lower values of n_{eu} which may be incompatible with required fusion performance, in particular the α-heating, although the connection between core and separatrix densities can be manipulated, e.g. by pellet fuelling.

Acknowledgment

The authors wish to thank Dennis Whyte and Rob Goldston for valuable discussions. This work was supported by the Collaborative Research Opportunities Grant from the National Sciences and Engineering Research Council of Canada and by the US Department of Energy under Cooperative Agreement No DE-FC02-04ER54698.

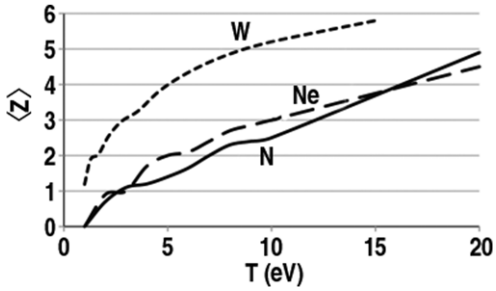

Figure A1. Average charge state: N (solid), Ne (long dashed), W (short dashed).

Appendix. Physical sputtering by low-temperature plasmas and prompt local deposition, reducing net erosion relative to gross erosion

For low-Z divertor targets the primary cause of physical sputtering is by D and T ions and neutrals. For mono-energetic $Z = 1$ ions accelerated through a sheath of potential drop $3kT_e$, $E_{impact} \sim 5\,kT$ (for $T_e = T_i$). Ions having a Maxwellian energy distribution far upstream of the target have a distribution that is roughly a Maxwellian at the target surface shifted by $\sim 3kT_e$. Emmert *et al* calculated the impacting energy distribution in detail for the case where the ions are accelerated collisionlessly in the pre-sheath and sheath, see figure 6 of [30]. One can then use the Emmert energy distribution to calculate the physical sputtering yield using the TRIM code calculations of Eckstein [8], integrating over the Emmert distribution and assuming 50 : 50 D : T. It will be shown in [31], however, that the sputtering yield calculated in this way differs rather little from that obtained assuming monoenergetic D and T ions of impact energy $5kT$ and therefore the latter, simpler assumption is made here.

Yields increase as the incidence becomes more glancing. The magnetic pitch angle at the divertor target is typically very small, a few degrees, and if this were the actual impact angle the increase in yield would be very large; however, the effect of the MPS is to turn the ions so that the typical impact angle is roughly 45°. At 45° the yield is only about twice the normal incidence yield [8]. The effect of surface roughness is to further improve the approximation that the representative incidence angle is about 45°. Thus a common practice in edge impurity modelling is to double the normal incidence yields [32] and we follow this here.

For high-Z PFCs, a low-Z impurity, such as N, Ne or Ar, has to be added at the %-level in order to dissipate power radiatively, in which case the dominant sputtering particle is the low-Z ion; the average ionization state of a low-Z ion in a plasma with $T_e \sim 10$ eV is $\langle Z \rangle \sim 3$,[3] see figure A1 which assumes coronal equilibrium. In principle, the average charge state can be higher because of ions coming from upstream, also it can be lower because of ionization times longer than the residence time; however, since N and Ne are added to the plasma in order to dissipate power that would otherwise be deposited on the targets by charged particles, it will be necessary to ensure that the N and Ne are injected in such a

[3] Los Alamos National Laboratory, atomic physics and plasma modeling codes. Available at the Amdis database, http://www-amdis.iaea.org/cgi-bin/EFFRATES/ss.pl

way that they are fairly dispersed spatially and not concentrated immediately in front of the targets, in which case the coronal equilibrium assumption provides an underestimate of $\langle Z\rangle$. The W case is discussed below.

An ion with charge Z accelerated through a sheath drop of $3kT$ has an impact energy of $\sim(3Z+2)kT$, not including the pre-sheath acceleration; however, the latter energy gain can be significant. If the plasma is highly collisional—the situation of interest here—then the impurity ion is accelerated, in the pre-sheath by frictional coupling with the majority DT ions, to essentially the DT sound speed at the sheath edge [33]. This *pre*-sheath energy gain is $\frac{1}{2}m_z c_{\mathrm{sDT}}^2 = (m_z/m_{\mathrm{DT}})kT$ which can be larger than the sheath energy gain. Thus in total

$$E_{\mathrm{impact}} \sim (2 + 3Z + m_Z/m_{\mathrm{DT}})kT. \tag{A1}$$

Inserting the values of $\langle Z\rangle$ from figure A1 into equation (A1) for Z gives the values of Y_{eff} shown in figure 1 for the W + N and W + Ne cases, using the Eckstein $Y(E_{\mathrm{impact}})$ values. Since the impurity ions have such high-directed energy relative to their random energy by the point where they strike the surface, the monoenergetic assumption is particularly good. The values of Y in figure 1 have been multiplied by 0.01 on the assumption that the flux of N or Ne is 1% of the DT-ion flux to the surface.

As can be seen in figure A1, the charge state of tungsten in *thermal equilibrium with the plasma* is rather high even for very low T, which would give a large sheath acceleration of W ions returning to the surface, increasing the self-sputtering yield. If the W ions are collisionally well coupled to the plasma then an even larger energy gain would occur, namely the pre-sheath energy gain of $(m_{\mathrm{W}}/m_{\mathrm{DT}})kT = 73.5kT$. Thus at $T = 10\,\mathrm{eV}$, $E_{\mathrm{impact\text{-}W}}$ would be of order 1 keV where the self-sputtering yield is $\sim$ unity [8], resulting in a sputtering runaway catastrophe. However, the assumption here is that the vast majority of the W particles sputtered from the divertor targets will promptly return to the solid surface due to their small gyro-radius, see below, and so the W ions will not be thermally and (momentum) collisionally well coupled to the DT ions. Therefore the effect of self-sputtering on Y_{eff}, which is to increase it by the multiplicative factor $1/(1 - Y_{\mathrm{self\text{-}sput}})$, has not been included in figure 1.

It should be noted that if the main walls are covered with W, then the W sputtered from those surfaces, e.g. by cx neutral impact, will not benefit from the effect of the MPS to cause prompt local deposition and when these ions eventually exit the plasma at some sheath—perhaps at the divertor targets—they may be well coupled collisionally to the DT plasma and could have high impact energy. Thus the *gross* erosion rate of W from the divertor targets may be quite high due to such *remote-source* W sputtering; however, assuming that the W sputtered from the targets—whether due to impact by W or the low-Z ions—is promptly deposited by gyro-motion, it can be still be the case that *net* erosion is very small.

The penetration distance of the sputtered neutrals is the ionization distance:

$$L_{\mathrm{ioniz}} = \frac{\sqrt{2\langle E_{Z_0}\rangle/m_{Z_0}}}{n_{\mathrm{t}}\langle\sigma v\rangle_{\mathrm{iz}}(T_{\mathrm{t}}, n_{\mathrm{t}})}, \tag{A2}$$

where $\langle E_{Z_0}\rangle$ is the average energy of the sputtered neutrals. For DT impact on C $\langle E_{C_0}\rangle$ was calculated assuming monoenergetic

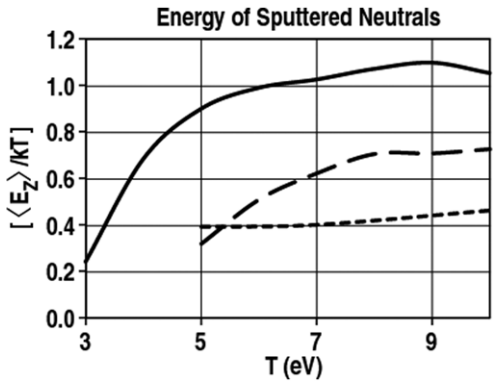

Figure A2. The average energy of sputtered neutrals [30]: Ne on W (solid), N on W (long dashed), DT on C (short dashed).

impacting DT ions and Y_{E}/Y values were taken from the Eckstein tables for 45° impact angle: $E_{Z_0} = E_{\mathrm{impact}}(Y_{\mathrm{E}}/Y)$. Details are given in [31]. The results are shown in figure A2.

The ionization rate coefficients are taken from ADAS [3]. For carbon the ADAS coefficients include density dependence. The ADAS coefficients for W are based on Loch *et al* [34] and do not as yet include density dependence. Values of L_{ioniz} for $n_{\mathrm{t}} = 10^{21}\,\mathrm{m}^{-3}$ are shown in figures A5–A7.

There are two different processes that can cause sputtered particles to experience prompt, local deposition, thereby reducing net erosion relative to gross erosion:

(a) deposition during the first gyro-orbit of the newly ionized sputtered neutral, see discussion in [15],
(b) the parallel forces, namely the strong electric field and the strong frictional coupling to the fuel ions flowing towards the target, in the MPS, quickly transporting the ionized impurities back to the target, see e.g. [14].

We now consider each of these processes in turn.

(a) Deposition during the first gyro-orbit. This is a strong effect when $L_{\mathrm{ioniz}} \ll \rho_z$, the impurity Larmor radius. The values for ρ_z shown in figures A5–A7 assumed $B = 5\,\mathrm{T}$ and used $\sqrt{2\langle E_{Z_0}\rangle/m_{Z_0}}$ for the impurity ion speed. As can be seen from figures A5 and A6, for these plasma conditions this effect can be expected to be quite strong for W, even if the W is twice ionized, although it will be rather weak at $n_{\mathrm{t}} = 10^{20}\,\mathrm{m}^{-3}$. For C, figure A7, this effect will be rather weak even at $n_{\mathrm{t}} = 10^{21}\,\mathrm{m}^{-3}$. Once the sputtered particles are ionized they return very quickly to the surface in approximately one half gyro-period, $\tau_{1/2\text{-gyro}} = \pi m_z/eB$, $\sim$0.079(1.2) μs for C (W) at $B = 5\,\mathrm{T}$.

(b) The strong parallel forces in the MPS. We start with the electric field force acting on the impurity ions in the MPS. In figure A3 the spatial variation of the electrostatic potential in the MPS taken from Chodura [13], for $\psi = 85°$, the angle between $\boldsymbol{B}$ and the normal to the target surface, is shown. The natural scale length of the MPS is the majority (i.e. fuel) ion Larmor radius:

$$\rho_{\mathrm{DT}} = \frac{\sqrt{2m_{\mathrm{DT}}kT_{\mathrm{t}}}}{eB}. \tag{A3}$$

Impurity neutrals that are ionized within the MPS experience the very strong parallel electric field of the MPS,

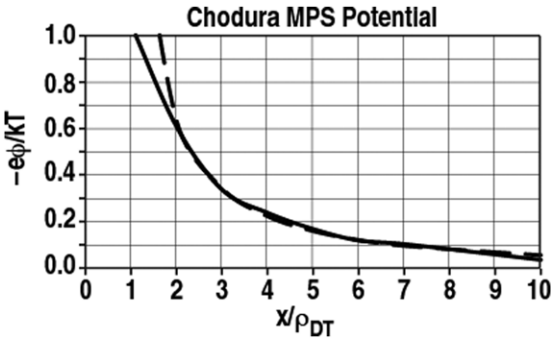

Figure A3. The electrostatic potential in the MPS from Chodura [13] for angle between B and the surface $\psi = 85^\circ$ (solid) and an approximate fit: $e\phi/kT\,(x/\rho_{\rm DT}) = 1.8(x/\rho_{\rm DT})^{-1.5}$ (dashed).

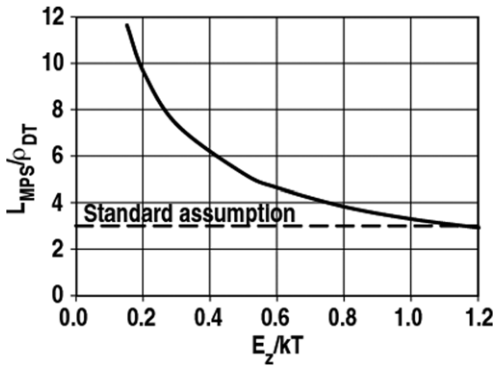

Figure A4. The effective thickness of the MPS with regard to escape of sputtered neutrals of energy E_z.

$E_{||}^{\rm MPS}$, which tends to promptly return them to the surface where they deposit out. An approximation is sometimes made that the thickness of the MPS is $\sim 3\rho_{\rm DT}$ to then compare with $L_{\rm ioniz}$ in order to decide whether this effect will be strong for promptly returning the sputtered particles locally. This approximation underestimates the effectiveness of this process when $\langle E_{Z_0}\rangle$ is small compared with $kT_{\rm t}$. Suppose the impurity neutrals were launched with, for example, $\langle E_{Z_0}\rangle = 0.2kT_{\rm t}$ directly in the parallel direction and against the direction of $E_{||}^{\rm MPS}$, then as can be seen from figure A3, provided this particle is ionized within a distance of $\sim 4\rho_{\rm DT}$ from the surface, it would not have sufficient kinetic energy to escape from the MPS potential well; thus the effective thickness of the MPS for prompt local deposition for this specific sputtered particle would be $\sim 4\rho_{\rm DT}$. The sputtered particles are launched with something like a cosine angular distribution and most of the particles do not have a large velocity in the anti-$E_{||}^{\rm MPS}$ direction, so that they are still more easily trapped. This situation has been modelled and details are given in [31]. Here we will use the results of that analysis without further elaboration. The main result is shown in figure A4, namely the effective thickness of the MPS for purposes of stopping all of the sputtered particles from escaping, due to $E_{||}^{\rm MPS}$ alone (ion–ion collisions, i.e. frictional drag between the impurity ion and the DT plasma flowing at $\sim$ sonic speed towards the surface, also contributes to the prompt deposition, below). The effective MPS thickness is a function of $\langle E_{Z_0}\rangle/kT_{\rm t}$. It can be shown that

$$\frac{L_{\rm MPS}}{\rho_{\rm DT}} \approx 3.28\left(\frac{E_{Z_0}}{kT_{\rm t}}\right)^{-2/3}, \qquad \text{(A4)}$$

which is the effective thickness of the MPS, $L_{\rm MPS}$, with regard to prompt, local deposition of sputtered particles due to $E_{||}^{\rm MPS}$.

As can be see from figure A4, when $E_{Z_0}/kT_{\rm t} \ll 1$, the effective thickness of the MPS is much higher than the fuel-ion Larmor radius. When $E_{Z_0}/kT_{\rm t} \sim 1$, on the other hand, the commonly used approximation of $L_{\rm MPS} \sim 3\rho_{\rm DT}$ [14, 35] is seen to be good. In figures A5–A7 the values for $L_{\rm MPS}$, ρ_z and $L_{\rm ioniz}$ are shown for comparison. As can be seen from figures A5 and A6, for tungsten both the $E_{||}^{\rm MPS}$ and ρ_z processes should be quite effective for $n_{\rm t} = 10^{21}\,{\rm m}^{-3}$ in causing prompt, local deposition. For carbon the ρ_z process will not be very effective but the $E_{||}^{\rm MPS}$ process is strong. At $n_{\rm t} = 10^{20}\,{\rm m}^{-3}$, however, neither process will be very effective for either element since $L_{\rm ioniz} \propto 1/n_{\rm t}$ while ρ_z and $L_{\rm MPS}$ are independent of $n_{\rm t}$.

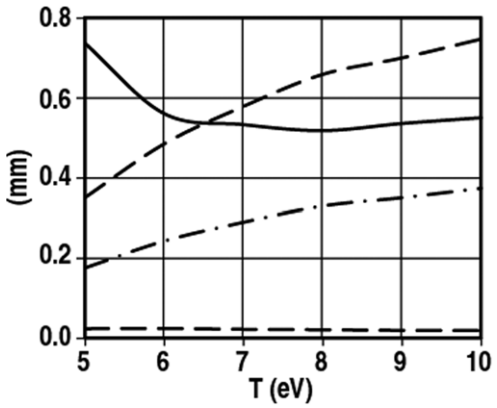

Figure A5. N on W; for $n_{\rm e} = 10^{21}\,{\rm m}^{-3}$ and $B = 5\,{\rm T}$; $L_{\rm MPS}$ (solid), $L_{\rm ioniz}$ (long dashed), ρ_z for W^+ (short dashed), ρ_z for W^{2+} (dotted–dashed).

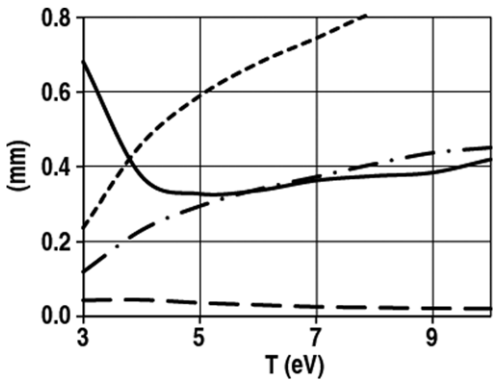

Figure A6. Ne on W; for $n_{\rm e} = 10^{21}\,{\rm m}^{-3}$ and $B = 5\,{\rm T}$; $L_{\rm MPS}$ (solid), $L_{\rm ioniz}$ (long dashed), ρ_z for W^+ (short dashed), ρ_z for W^{2+} (dotted–dashed).

We consider next the possibility of prompt, local deposition resulting from the frictional force between the impurity ions and the DT ions which move at speed $\sim c_{\rm sDT}$ towards the target. As can be seen in figures A5–A7, for $n_{\rm t} \sim 10^{21}\,{\rm m}^{-3}$ and $T_{\rm t} \sim 5\,{\rm eV}$, the sputtered neutrals will be ionized within the MPS. The motion of the DT ions within the MPS is rather complicated but to a first approximation the DT-ion flow speed is constant at the sound speed, $c_{\rm sDT}$, but turns from being along $\boldsymbol{B}$ at the MPS entrance to being normal to the solid surface at the MPS exit, i.e. entrance to the DS.

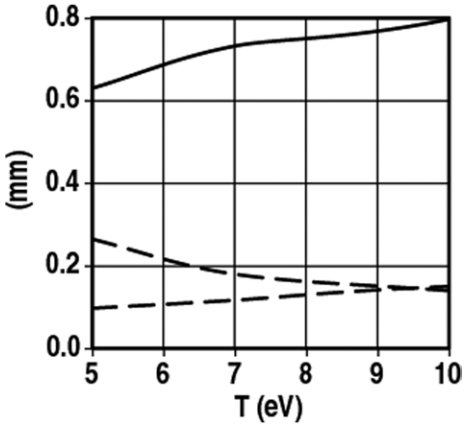

Figure A7. DT on C; for $n_e = 10^{21}\,m^{-3}$ and $B = 5\,T$; L_{MPS} (solid), L_{ioniz} (long dashed), ρ_z for C^+ (short dashed).

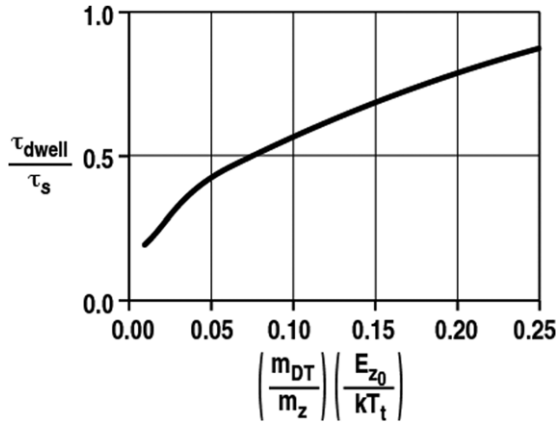

Figure A8. The normalized dwell time of an impurity ion in the plasma when controlled by friction in the MPS, τ_{dwell}/τ_s, as a function of the lumped parameter $(m_{DT}/m_Z)(E_{Z_0}/kT_t)$.

The frictional force dragging the impurity ions towards the solid surface is quite strong; however, because of the change in the flow direction of the DT ions it is much more difficult to analyse than was the case of the electric field force on the impurity ions (above) which essentially involves only energy conservation. Here we will obtain an underestimate of the effect of the friction force by assuming that it remains in the $\boldsymbol{B}$-direction all the way to the solid surface. This constitutes an underestimate since in reality the frictional force on the impurity ions acts to transport them by a shorter, quicker route to the surface than the parallel-to-$\boldsymbol{B}$ route.

By way of further underestimating the strength of this effect we will assume that the sputtered neutral velocity is precisely in the $\boldsymbol{B}$-direction away from the surface, with initial ion velocity $v_{Z||0} = (2\langle E_{Z_0}\rangle/m_Z)^{1/2}$. The parallel velocity of the impurity ion controlled by frictional coupling to the DT-ion flow at speed c_{sDT} is given by

$$m_Z \frac{dv_{Z||}}{dt} = \frac{m_Z(-c_{sDT} - v_{Z||})}{\tau_s}, \qquad \text{(A5)}$$

where the positive direction is away from the surface and τ_s is the DT–Z ion collisional stopping time. The solution to equation (A5) gives the dwell time of the impurity ion, τ_{dwell}, before striking the solid surface:

$$\frac{\tau_{dwell}}{\tau_s} = \frac{L_{ioniz}}{c_{sDT}\tau_s} + \left(1 + \left(\frac{m_{DT}}{m_Z}\right)^{1/2}\left(\frac{E_{Z_0}}{kT_t}\right)^{1/2}\right)(1 - e^{-\tau_{dwell}/\tau_s}). \qquad \text{(A6)}$$

For the typical conditions considered here it is readily shown that the first term on the rhs of equation (A6) is small compared with the second one and we will neglect it here. Figure A8 then gives τ_{dwell}/τ_s as a function of the single lumped parameter $(m_{DT}/m_Z)(E_{Z_0}/kT_t)$. Example: carbon and $(E_{Z_0}/kT_t) = 0.4$ for which $\tau_{dwell}/\tau_s = 0.531$. The stopping time is given, e.g. by equation (6.35) of [5]:

$$\tau_s = \frac{1.47 \times 10^{13} m_Z T_{DT}(T_{DT}/m_{DT})^{1/2}}{(1 + m_{DT}/m_Z) n_{DT} Z^2 \ln\Lambda}, \qquad \text{(A7)}$$

for $n(m^{-3})$, $T(eV)$, $m(amu)$, $\tau(s)$. Thus for $n_t = 10^{21}\,m^{-3}$ and $T_t = 5\,eV$, $\tau_s = 1.56 \times 10^{-7}\,s$ and $\tau_{dwell} = 8.28 \times 10^{-8}\,s$.

A criterion is needed to define whether the deposition is to be considered to be *prompt, local*. The practical point is that if net erosion is to be made much less than gross erosion then the cross-field step that occurs while the impurity is in the plasma should be as short as possible. The concept of prompt, local deposition was originally applied to the case where the deposition occurs during the first gyro-orbit and was considered as something that applied to high-Z elements, e.g. W, only. In that case the cross-field step is approximately the gyro-radius which, as can be seen from figures 5 and 6, is ~0.5mm for W^+ for the currently considered plasma conditions. In the cases where the deposition is due to the electric field or the frictional force in the MPS we might take the cross-field step to be $\sim\sqrt{2D_\perp\tau_{dwell}}$. For the same example and assuming $D_\perp = 1\,m^2\,s^{-1}$ this gives a cross-field step of ~0.4 mm, which therefore indicates *prompt, local* deposition as traditionally understood. For typical attached divertor conditions in present tokamaks, e.g. $n_t \sim 2 \times 10^{19}\,m^{-3}$ and $T_t \sim 20\,eV$, then $\tau_s = 4.1 \times 10^{-5}\,s$ and $\sqrt{2D_\perp\tau_{dwell}} = 6.1\,mm$, which cannot be considered to be local, prompt deposition. (For such conditions the ionization of the sputtered neutral is also not within the MPS; however, the DT-ion flow speed is still $\sim c_{sDT}$ along $\boldsymbol{B}$ for some distance beyond the MPS.)

It would be useful if it were possible to readily show quantitatively what the expected net erosion rate would be in a power reactor for the plasma conditions of figures A5–A7. Unfortunately this is not possible without (i) making detailed assumptions about the spatial variation of n_e and T_e across the divertor strike points and then (ii) carrying out detailed impurity transport analysis since the actual net erosion rate will depend almost entirely on the details. The net erosion for the indicated conditions will depend primarily on the non-typical sputtered particles, such as the ones in the high-energy tail of the sputtered neutral (Thompson) energy distribution, and such as the ones sputtered from the periphery of the plasma 'footprint' on the divertor targets where escape from the prompt local deposition processes can occur. Power reactors may also require slow magnetic sweeping of the divertor strike point locations so as to further reduce net erosion and that useful but complicating process should also be included in any worthwhile quantitative analysis of the annual net erosion in power reactors. It will be valuable to make such estimates; however, it will require analysis and a further report of comparable magnitude to the present one.

References

[1] Lackner K. 1994 *Comments Plasma Phys. Control. Fusion* **15** 359
[2] Hutchinson I.H and Vlases G.C. 1996 *Nucl. Fusion* **36** 783
[3] Summers H. P. 2004 *The ADAS User Manual* version **2.6** http://www.adas.ac.uk
[4] Kotschenreuther M., Valanju P.M., Mahajan S.M. and Wiley J.C. 2007 *Phys. Plasmas* **14** 072502 (see discussion in appendix A)
[5] Stangeby P.C. 2000 *The Plasma Boundary of Magnetic Fusion Devices* (Bristol: Institute of Physics Publishing)
[6] Konishi S. and Ueda Y. 2008 Japan PFC/divertor concepts for power plants *Int. HHFC Workshop on Readiness to Proceed from Near Term Fusion Systems to Power Plants (10–12 December 2008)* University of California San Diego http://aries.ucsd.edu/raffray/IHHFC/program.html
[7] Baldwin M.J., Doerner R.P., Nishijima D., Tokunaga K. and Ueda Y. 2009 *J. Nucl. Mater.* **390–391** 886
[8] Eckstein W. 2002 Calculated sputtering, reflection and range values *Report* IPP 9/32
[9] Najmabadi F. and The ARIES Team 2006 *Fusion Eng. Des.* **80** 3
[10] Whyte D.G. 2005 *Fusion Sci. Technol.* **48** 1096
[11] Kotschenreuther M., Valanju P. and Mahajan S. 2007 *Proc. 9th Meeting of APS Division of Plasma Physics (Orlando, FL) Bull. Am. Phys. Soc.* **52** 125 http://meetings.aps.org/Meeting/MAR07/Content/662
[12] Ryutov D.D. 2007 *Phys. Plasmas* **14** 064502
[13] Chodura R. 1982 *Phys. Fluids* **25** 1626
[14] Brooks J.N. 1990 *Phys. Fluids* B **2** 1858
[15] Naujoks D. *et al* 1996 *Nucl. Fusion* **36** 671
[16] Kocan M. and Gunn J.P. 2010 *Plasma Phys. Control. Fusion* **52** 045010
[17] Lisgo S. *et al* 2005 *J. Nucl. Mater.* **337–339** 139
[18] Igitkhanov Yu.L. 1988 *Contrib. Plasma Phys.* **28** 477
[19] Kallenbach A., Asakura N., Kirk A., Korotkov A., Mahdavi M.A., Mossessian D. and Porter G.D. 2005 *J. Nucl. Mater.* **337–339** 381
[20] Krasheninnikov S.I. 1994 *Contrib. Plasma Phys.* **34** 151
[21] Stangeby P.C., Canik J.M. and Whyte D.G. 2010 The relation between upstream density and temperature widths in the scrape-off layer and the power width in an attached divertor *Nucl. Fusion* **50** 125003
[22] Whyte D.G. 2009 Relating upstream and divertor power widths *Presentation at Plasma Science & Fusion Center* (Cambridge, MA: MIT) http://www.psfc.mit.edu/library1/catalog/online_pubs/presentations/power_width_relation.pdf
[23] Goldston R.J. *et al* 2009 An initiative to tame the plasma material interface, http://www.fusion.ucla.edu/FNST/Renew_Presentations/Wednesday/7.4-Goldston-NHTX%20for%20ReNeW.pdf
[24] Loarte A. *et al* 1999 *J. Nucl. Mater.* **266–269** 587
[25] Kirnev G., Fundamenski W. and Corrigan G. 2007 *Plasma Phys. Control. Fusion* **49** 689
[26] Carlstrom T.N., Hsieh C.L., Stockdale R.E., Nilson D.G. and Hill D.N. 1997 *Rev. Sci. Instrum.* **68** 1195
[27] Leonard A.W. *et al* 1997 *Phys. Rev. Lett.* **78** 4769
[28] Leonard A.W. *et al* 1998 *Phys. Plasmas* **5** 1736
[29] Leonard A.W., Meyer W.H., Geer B., Behne M. and Hill D.N. 1995 *Rev. Sci. Instrum.* **66** 1201
[30] Emmert G.A. *et al* 1980 *Phys. Fluids* **23** 803
[31] Stangeby P.C. 2011 Strong suppression of net erosion at divertor targets due to prompt local deposition caused by the strong electric field of the magnetic pre-sheath, in preparation
[32] Eckstein W. 2006 private communication, IPP, Garching
[33] Stangeby P.C. 1987 *J. Phys. D: Appl. Phys.* **20** 1472
[34] Loch S.D. *et al* 2005 *Phys. Rev.* A **72** 052716
[35] Kirschner A., Phillips V., Winter J. and Kogler U. 2000 *Nucl. Fusion* **40** 989